HEALTH AND MEDICINE

Three-dimensional heart extracellular matrix enhances chemically induced direct cardiac reprogramming

Yoonhee Jin[1,2]†, Hyeok Kim[3,4]†, Sungjin Min[1], Yi Sun Choi[1], Seung Ju Seo[2], Eunseon Jeong[1], Su Kyeom Kim[1], Hyang-Ae Lee[5], Sung-Hyun Jo[6], Jae-Hyun Park[3,4], Bong-Woo Park[3,4], Woo-Sup Sim[3,4], Jin-Ju Kim[3,4], Kiwon Ban[7], Yun-Gon Kim[6], Hun-Jun Park[3,4,8]*, Seung-Woo Cho[1,9,10]*

Direct cardiac reprogramming has emerged as a promising therapeutic approach for cardiac regeneration. Full chemical reprogramming with small molecules to generate cardiomyocytes may be more amenable than genetic reprogramming for clinical applications as it avoids safety concerns associated with genetic manipulations. However, challenges remain regarding low conversion efficiency and incomplete cardiomyocyte maturation. Furthermore, the therapeutic potential of chemically induced cardiomyocytes (CiCMs) has not been investigated. Here, we report that a three-dimensional microenvironment reconstituted with decellularized heart extracellular matrix can enhance chemical reprogramming and cardiac maturation of fibroblasts to cardiomyocytes. The resultant CiCMs exhibit elevated cardiac marker expression, sarcomeric organization, and improved electrophysiological features and drug responses. We investigated the therapeutic potential of CiCMs reprogrammed in three-dimensional heart extracellular matrix in a rat model of myocardial infarction. Our platform can facilitate the use of CiCMs for regenerative medicine, disease modeling, and drug screening.

INTRODUCTION

Cardiac injury in adults results in irreversible loss of cardiomyocytes followed by the formation of fibrotic scar tissue. Direct cellular reprogramming offers an attractive option to generate functional cardiomyocytes. It was reported that direct reprogramming of somatic cells into cardiomyocytes can be achieved in vitro and in vivo by forced expression of transcription factors (TFs) and/or microRNAs (1–4). More recently, combinations of small molecules were applied to directly reprogram fibroblasts into cardiomyocyte-like cells (5–7). TF- and microRNA-mediated direct reprogramming of fibroblasts into cardiomyocytes promotes functional recovery of the infarcted heart (8–12). Although TF gene delivery with viral vectors has been effective in cardiac reprogramming, viral methods are not favorable in clinical settings (13). As an alternative, small-molecule compounds can be used to produce chemically induced cardiomyocyte (CiCM)–like cells from fibroblasts (14–17). Small molecules have also been applied in combination with TF gene delivery to enhance the efficiency of direct cardiac reprogramming (18). Chemical reprogramming has distinct advantages that make it amenable to clinical development as it is less immunogenic and tumorigenic than viral reprogramming. In addition, chemical methods are usually more rapid and reversible than genetic methods. The efficiency of chemically induced direct reprogramming in vitro is relatively modest, however, and new approaches beyond simple two-dimensional (2D) cell culture are needed. It is currently unknown how 3D microenvironments affect the reprogramming of fibroblasts into CiCMs. In addition, the therapeutic potential of CiCMs has not been investigated in infarcted hearts.

The importance of biochemical and biophysical microenvironmental cues during the direct reprogramming process has been demonstrated (19–21). Several studies reported that biophysical cues from the extracellular matrix (ECM) and substrate topography play important roles in cardiac differentiation of pluripotent stem cells or cardiac progenitor cells and in direct cardiac reprogramming (22, 23). Li et al. (22) demonstrated that 3D culture of fibroblasts in fibrin hydrogel improved the efficiency of microRNA-mediated direct cardiac reprogramming. We previously reported that tissue-specific 3D ECM improved TF-mediated direct neuronal reprogramming (19).

Here, we demonstrate that decellularized heart ECM (HEM) in a 3D hydrogel format improves chemically induced direct reprogramming of fibroblasts into CiCMs, which exhibit improved cardiac structural and functional maturation compared with CiCMs reprogrammed in other formats. Compared with conventional 2D ECM [i.e., Matrigel (MAT)], the heart-mimetic 3D microenvironment not only increased the cardiac conversion efficiency but also induced more mature phenotypes as indicated by sarcomeric organization, synchronized spontaneous beating, and regular calcium transients. Transplantation of 3D HEM CiCMs into a rat model of myocardial infarction (MI) resulted in improved cardiac contractibility and reduced fibrosis. Our results suggest that

[1]Department of Biotechnology, Yonsei University, Seoul 03722, Republic of Korea. [2]Department of Physiology, Yonsei University College of Medicine, Seoul 03722, Republic of Korea. [3]Department of Biomedicine and Health Sciences, The Catholic University of Korea, Seoul 06591, Republic of Korea. [4]Division of Cardiology, Department of Internal Medicine, Seoul St. Mary's Hospital, The Catholic University of Korea, Seoul 06591, Republic of Korea. [5]Korea Institute of Toxicology, Korea Research Institute of Chemical Technology, Daejeon 34114, Republic of Korea. [6]Department of Chemical Engineering, Soongsil University, Seoul 06978, Republic of Korea. [7]Department of Biomedical Sciences, City University of Hong Kong, Kowloon 999077, Hong Kong. [8]Cell Death Disease Research Center, College of Medicine, The Catholic University of Korea, Seoul 06591, Republic of Korea. [9]Center for Nanomedicine, Institute for Basic Science (IBS), Seoul 03722, Republic of Korea. [10]Graduate Program of Nano Biomedical Engineering (NanoBME), Advanced Science Institute, Yonsei University, Seoul 03722, Republic of Korea.
*Corresponding author. Email: seungwoocho@yonsei.ac.kr (S.-W.C.); cardioman@catholic.ac.kr (H.-J.P.)
†These authors contributed equally to this work.

microenvironmental cues from the 3D HEM have pivotal effects on the generation of therapeutic CiCMs.

RESULTS

HEM contains a wide range of proteins that are important for heart development

HEM was prepared through decellularization and subsequent solubilization of porcine heart tissue. Cellular components were removed from the heart tissue by serial chemical treatments with the ionic detergent SDS and the nonionic detergent Triton X-100. It has been reported that SDS yields decellularized cardiac tissue more efficiently compared to Triton X-100 (24). However, SDS tends to harshly disrupt the tissue structure and damage the ECM, and thus, a combination of the two detergents has been preferable for ideal decellularization. A protocol that combines both detergents has been reported to produce the most well-preserved decellularized cardiac ECM in terms of glycosaminoglycan (GAG), collagen, and other noncollagenous proteins with the lowest amount of DNA (25). We further optimized this reported method to effectively yield decellularized heart tissue with well-preserved ECM components by adjusting the times and intervals of detergent treatments. Hematoxylin and eosin staining for DNA quantification (fig. S1, A and B) before and after the decellularization process confirmed that most of the cells were removed from the decellularized heart tissue. DNA quantification assay of three batches of HEM used in our study revealed that an average of 4.89, 13.4, and 4.40 ng of double-stranded DNA (dsDNA; per milligram of HEM in dry weight) was detected in batches 1, 2, and 3, respectively (fig. S1B). Given that the remaining DNA content in decellularized tissue–derived ECM should be below 50 ng of dsDNA per milligram of ECM in dry weight for ensuring the safety (26), these results support that our HEM samples are safe to be used for in vivo applications. Masson's trichrome (MT) staining for collagen quantification (fig. S1, C and D) and Alcian blue staining for GAG quantification (fig. S1, E and F) showed that collagen and GAG contents were well preserved after the decellularization process.

The protein contents of the prepared HEM and MAT, the most widely used matrix for cardiac culture, were determined by mass spectrometry (MS) and compared with those of human heart tissue (Fig. 1) (27). Comparison to the matrisome database of ECM and ECM-associated proteins (28) showed that 50.8 and 88.4% of the proteins in HEM and MAT, respectively, were matrisome proteins, whereas only 4.8% of the proteins in human heart tissue were matrisome proteins (Fig. 1A). A total of 76 matrisome proteins (59 core matrisome proteins and 17 matrisome-associated proteins) were identified in the HEM (table S1). Although the percentages vary, we found that HEM and native heart tissue both contain abundant collagens, glycoproteins, and proteoglycans (Fig. 1B). On the other hand, 97.6% of the matrisome proteins identified in MAT were glycoproteins. A majority of the matrisome proteins detected in HEM (73 of 76 ≈ 96.1%) overlapped with the matrisome proteins identified in native heart tissue (Fig. 1C). Seven and 4 of the 10 most abundant core matrisome proteins (all collagens, glycoproteins, or proteoglycans) in the HEM and MAT, respectively, were also among the most abundant core matrisome proteins in native heart tissue (Fig. 1D). This suggests that HEM contains cardiac-like structural and matricellular components.

We next compared the proteins (matrisomal and non-matrisomal) expressed in native heart tissue, HEM, and MAT to a list of proteins with at least four times higher expression in the heart than in other organs (29). We found that heart-enriched proteins accounted for 37.9, 22.7, and 0.1% of the total protein expression in native heart tissue, HEM, and MAT, respectively (Fig. 1E). In total, 64 and 21 different heart-enriched proteins were identified in HEM and MAT, respectively (Fig. 1F). Only 1 heart-enriched protein was identified exclusively in MAT, whereas 44 heart-enriched proteins were found exclusively in HEM. Gene ontology biological process (GOBP) analysis of the heart-enriched proteins found exclusively in HEM indicated that those proteins play roles in muscle contraction and development (Fig. 1G).

We next assessed the differences between the protein profiles of MAT and HEM (Fig. 1, H to K). A volcano plot demonstrates the differential abundances of all the proteins identified in HEM and MAT (Fig. 1H). Thirty-three core matrisome proteins were more abundant (≥2-fold, $P < 0.05$) in HEM than in MAT, whereas 10 core matrisome proteins were more abundant in MAT than in HEM (Fig. 1I). HEM contained core matrisome proteins that are important for normal heart development, including collagen types VI and XI, elastin, fibronectin, versican, decorin, and lumican (30–33). GOBP enrichment analysis revealed that the proteins identified only in MAT are involved in peptide and nitrogen-compound biosynthetic and metabolic processes, whereas those identified only in HEM are involved in muscle development, organization, and contraction (Fig. 1, J and K). After reduction of redundant GO terms, the terms "muscle contraction," "regulation of muscle contraction," "muscle structure development," and "supramolecular fiber organization" were substantially enriched among the HEM proteins but not among the MAT proteins. Together, the proteomic data indicate that HEM contains essential components related to heart development and function that are absent in MAT.

Decellularized heart tissue is solubilized with pepsin treatment for HEM hydrogel preparation. As pepsin treatment under acidic condition [hydrochloric acid (HCl)] may affect the ECM contents, we performed proteomic analysis of the HEM samples before and after solubilization with pepsin (fig. S2). We found that the profiles of ECM proteins in the lyophilized HEM (before pepsin treatment) and solubilized HEM (pregel solution after pepsin treatment) were similar (50 to 55% matrisome proteins and 45 to 50% nonmatrisome proteins; fig. S2A). The overall compositions of matrisome proteins were also similar to each other, except that the contents of collagens decreased and glycoprotein contents increased in the HEM pregel solution, as compared to the lyophilized HEM sample (fig. S2B). Out of 88 matrisome proteins detected in the HEM pregel solution, 65 proteins overlapped with the proteins detected in the lyophilized HEM (fig. S2C). Comparison of the top 10 core matrisome proteins with the highest intensity based on absolute quantification (iBAQ) values revealed that 9 of 10 proteins overlapped in the lyophilized HEM sample and HEM pregel solution (red-highlighted ones; fig. S2D). Lyophilized HEM and HEM pregel solution showed 22.7 and 15% heart-enriched protein expression of the total protein expression, respectively (fig. S2E). In total, 64 and 52 heart-enriched proteins were identified in the lyophilized HEM sample and HEM pregel solution, respectively, and 43 proteins were commonly detected in these two samples (fig. S2F). Together, HEM solubilization process with pepsin
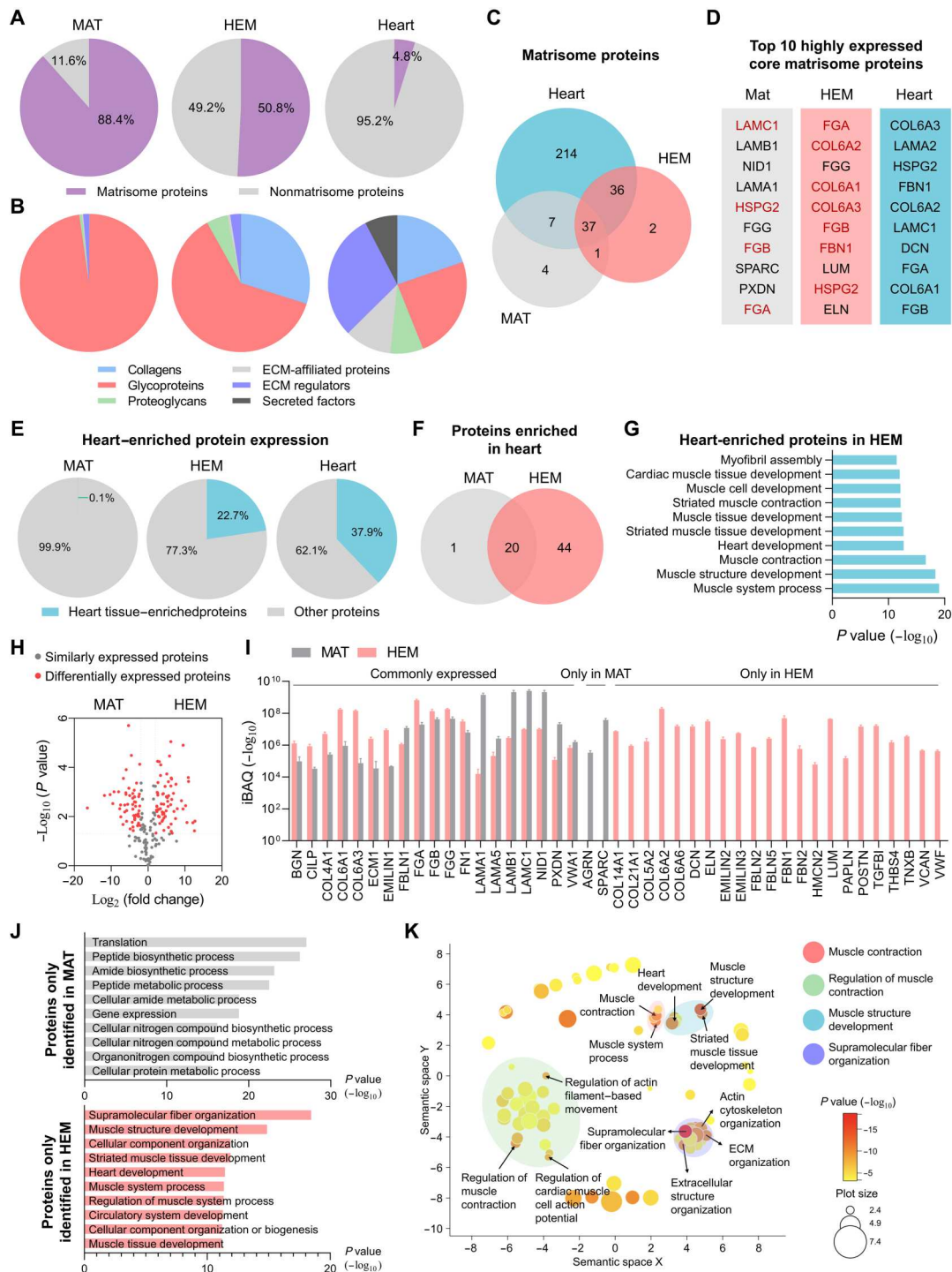
Fig. 1. Protein identification and functional enrichment of HEM. (**A** and **B**) The relative expression of (A) matrisome and nonmatrisome proteins and (B) subtypes of matrisome proteins in HEM (n = 3), MAT (n = 3), and native heart. (**C**) Venn diagrams showing the numbers of the native heart–expressed matrisome proteins identified in MAT and HEM. (**D**) The top 10 core matrisome proteins that were the most abundant in MAT, HEM, and heart tissue. Proteins identified in MAT and HEM that overlap with the proteins in native heart are marked in red color. (**E**) The relative expression in MAT, HEM, and heart tissue of proteins known to be expressed at least four times more in heart tissue than in other organs (heart-enriched proteins). (**F**) The numbers of heart-enriched proteins identified in MAT and HEM. (**G**) The top 10 GOBP terms of heart-enriched proteins found in HEM but absent in MAT. (**H**) Volcano plot depicting the total protein expression in HEM relative to that in MAT. Red dots indicate significantly differentially expressed proteins with fold change ≥ 2 and $P < 0.05$. (**I**) Core matrisome proteins with different abundances in HEM and MAT (fold change ≥ 2, $P < 0.05$). (**J**) The top 10 enriched GOBP terms of proteins with the lowest P values identified only in MAT or HEM. (**K**) A semantic plot of the GOBP terms commonly enriched among the HEM-specific proteins. The positions of GOBP terms represent semantic similarities calculated by REVIGO (http://revigo.irb.hr/). The color indicates the P value, and the circle size indicates the frequency of the GO term in the Gene Ontology Annotation database (whole UniProt), with more general terms given larger size.

treatment does not seem to notably alter ECM profiles in the resultant HEM pregel solution, and matrisome and nonmatrisome proteins critical for cardiac reprogramming are mostly well preserved after solubilization.

For 3D HEM hydrogel formation, the pH of the HEM pregel solution was neutralized, and its salt concentration was balanced to isotonic condition. Although our protocol for HEM hydrogel preparation does not involve any purification steps to eliminate pepsin nor salts in the pregel solution, inactivated pepsin and balanced salts in 3D HEM hydrogel are not likely to interrupt the reprogramming process and affect cell viability. Actually, gelation protocols of decellularized tissue ECM through the pepsin-based solubilization process have been widely used with no extraction or purification step in numerous studies (34), and accordingly, tissue ECM hydrogels prepared by our gelation method have been identified as highly biocompatible scaffolds. Nonetheless, the purification steps to eliminate pepsin and salts (e.g., dialysis) may need to be considered for clinical setting in the future.

The mechanical property of the HEM hydrogel was compared with that of MAT by measuring the elastic modulus of each hydrogel. We found that MAT has a higher elastic modulus than HEM hydrogel (101.2 ± 2.49 Pa for MAT and 27.4 ± 2.48 Pa for HEM; fig. S3). Although MAT has greater elastic modulus than HEM hydrogel, the levels of mechanical properties of both hydrogels (~100 Pa) are far below that of native cardiac tissue (approximately 40 kPa in the case of 1-day postnatal mouse ventricle) (35), which may suggest that the difference in the mechanical properties between MAT and HEM hydrogel is too small to affect the reprogramming process. Thus, we assume that the improvements observed in HEM over MAT are mainly due to the biochemical cues rather than the mechanical cues. Nonetheless, the effect of mechanical cues provided by the HEM hydrogel needs to be more carefully investigated in the future study.

The 3D cardiac-specific ECM environment enhances cardiac reprogramming efficiency

HEM and MAT were applied for surface coating of culture substrates (2D HEM or 2D MAT) and for 3D hydrogel formation via temperature-mediated self-assembly of ECM proteins (3D HEM or 3D MAT). Primary mouse embryonic fibroblasts (PMEFs) were seeded on the 2D substrates or in the 3D hydrogels and treated with a combination of small molecules (Forskolin, CHIR99021, A83-01, and SC-1) after 4 hours of seeding or encapsulation (Fig. 2A). Forskolin increases the adenylyl intracellular levels of cyclic adenosine monophosphate (36). CHIR99021 inhibits glycogen synthase kinase 3β that leads to WNT activation (37). A83-01 suppresses activin/NODAL/transforming growth factor–β (TGF-β) by inhibiting activin receptor–like kinases 5, 4, and 7 (38). SC-1 inhibits Ras guanosine triphosphatase–activating protein and extracellular signal–regulated kinase 1 that leads to self-renewal and block differentiation (39). Four hours after cell seeding on 2D substrates (2D MAT and 2D HEM) or cell encapsulation into 3D hydrogels (3D MAT and 3D HEM), staining for cytoskeleton [filamentous actin (F-actin)] and focal adhesion (vinculin) showed that PMEFs adhered and started spreading out in both 2D and 3D conditions (fig. S4). The levels of cell adhesion and spreading seem sufficient to be activated in the early phase of reprogramming.

The cells seeded in 3D HEM or 3D MAT formed beating CiCM clusters as early as 3 days after chemical treatment (Fig. 2B and movies S1 and S2). By contrast, the cells seeded on 2D HEM or 2D MAT formed beating clusters on days 6 to 8 after chemical treatment at the earliest (Fig. 2B, fig. S5, and movies S3 and S4). We measured the elastic modulus as a representative mechanical property of the cardiac constructs in HEM or MAT. At 1 day of culture, the elastic modulus of the 3D HEM constructs was significantly higher (141.3 ± 9.7 Pa) than that of the 3D MAT constructs (69.7 ± 8.7 Pa; Fig. 2C). The average elastic modulus of the 3D HEM constructs increased to 1130.2 ± 336.8 Pa on day 5 of culture, whereas that of the 3D MAT constructs was unchanged. This suggests that the contractile cells in 3D HEM caused more mechanical stress, leading to the stiffening of the surrounding matrix, than the contractile cells in 3D MAT (40).

We investigated the efficiency of chemical cardiac reprogramming in each ECM condition (2D HEM, 2D MAT, 3D HEM, and 3D MAT) by analyzing the expression of cardiac proteins [α-actinin and cardiac troponin-T (cTnT)] and genes (Mef2c, Myh7, and Nkx2-5) 5 and 10 days after chemical treatment (Fig. 2, D to F). On day 5, α-actinin⁺ and cTnT⁺ cells with clear cross-striated patterns started to appear in the 2D HEM, 3D MAT, and 3D HEM cultures, with the 3D HEM cultures showing the highest numbers of cells with sarcomere structures (Fig. 2D). Quantitative real-time polymerase chain reaction (qPCR) analysis on days 5 and 10 revealed substantial increases in Mef2c, Myh7, and Nkx2-5 expression in all four chemically induced groups compared with untreated fibroblasts (Fig. 2, E and F). On day 5, the expression of Mef2c in the 3D MAT and 3D HEM cultures was almost two times higher than in the 2D MAT cultures (Fig. 2E). The expression of Myh7 was approximately two times higher in the 2D HEM and 3D MAT cultures and five times higher in the 3D HEM cultures compared with that in the 2D MAT cultures. Similarly, the expression of Nkx2-5 was 3 times higher in the 2D HEM and 3D MAT cultures and 30 times higher in the 3D HEM cultures compared with that in the 2D MAT cultures. Cardiac marker expression in all four chemically treated groups was further increased on day 10 after small-molecule treatment (Fig. 2F). The 3D HEM cultures showed the highest expression of cardiac markers on both days 5 and 10 (Fig. 2, E and F). Compared to the levels in neonatal cardiomyocytes, Actc1 and Myh7 expression were comparable in the 3D HEM CiCMs, whereas other CiCM groups showed significantly lower levels (fig. S6). The cTnT expression was significantly lower in all CiCM groups, whereas Scn5a expression was higher in 3D CiCM groups than in neonatal cardiomyocytes. We evaluated the cardiac conversion efficiency on day 7 after chemical treatment by flow cytometry (Fig. 2, G to J). The percentages of cTnT⁺ and α-actinin⁺ cells were highest in the 3D HEM cultures (48.7 ± 1.29% cTnT⁺ and 57.3 ± 0.58% α-actinin⁺; Fig. 2, G and I). The 2D MAT cultures showed the lowest cardiac conversion efficiency (9.5 ± 0.2% cTnT⁺ and 30.3 ± 0.58% α-actinin⁺). Immunocytochemical staining of the cells on day 7 also indicated that the 3D HEM cultures had higher cTnT⁺ and α-actinin⁺ expression (Fig. 2, H and J). The frequency of CiCMs with well-organized sarcomeric structures was highest in the 3D HEM cultures, whereas the other cultures contained mixed populations of CiCMs with and without sarcomeric structures (Fig. 2J).

We also checked the proliferative ability of CiCMs in 3D HEM hydrogel during reprogramming. We found that some of the cell
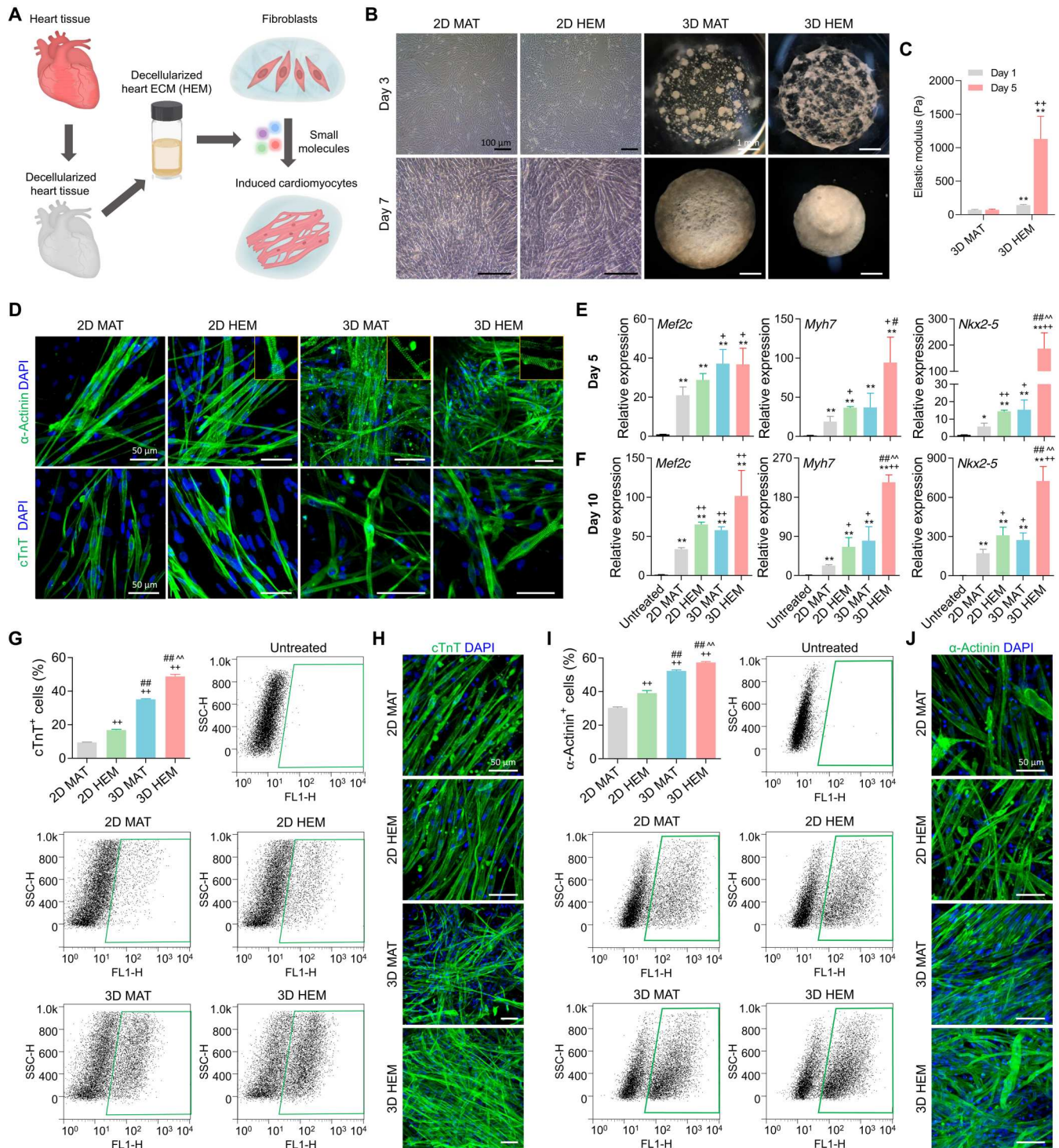
Fig. 2. The use of 3D HEM enhanced the efficiency of chemically induced direct cardiac reprogramming. (**A**) Schematic illustration of chemically induced direct cardiac reprogramming using decellularized heart–derived ECM. (**B**) Bright-field images of cells cultured on MAT- or HEM-coated 2D substrate or in MAT or HEM 3D hydrogel 3 and 7 days after chemical treatment [scale bars, 100 μm (black) and 1 mm (white)]. (**C**) Average elastic moduli of 3D MAT and 3D HEM constructs on days 1 and 5 of culture ($n = 4$; **$P < 0.01$ versus 3D MAT at the same time point, ++$P < 0.01$ versus corresponding 3D ECM at day 1). (**D**) Immunostaining for α-actinin and cTnT after 5 days of chemical treatment (scale bars, 50 μm). DAPI, 4′,6-diamidino-2-phenylindole. (**E** and **F**) Cardiac gene expression in untreated fibroblasts and cells in 2D MAT, 2D HEM, 3D MAT, or 3D HEM determined by qPCR on (E) day 5 and (F) day 10 after chemical treatment ($n = 3$). (**G**) Comparison of cTnT⁺ cells in each group analyzed by flow cytometry ($n = 3$) and (**H**) immunostaining on day 10 (scale bars, 50 μm). (**I**) Quantification of α-actinin⁺ cells by flow cytometry ($n = 3$) and (**J**) immunostaining on day 10 (scale bars, 50 μm). (E, F, G, and I) All data are expressed as the means ± SD. Statistical difference between the groups was determined by two-tailed t test (*$P < 0.05$ and **$P < 0.01$ versus untreated, +$P < 0.05$ and ++$P < 0.01$ versus 2D MAT, #$P < 0.05$ and ##$P < 0.01$ versus 2D HEM, and ^^$P < 0.01$ versus 3D MAT).

clusters in 3D HEM showed spontaneous beating as early as 3 days after chemical treatment for reprogramming (Fig. 2B). It seems that those cell populations were reprogrammed to cardiac lineage at days 3 to 7, while other populations were still under the reprogramming process. As some molecules used for chemical reprogramming (e.g., CHIR99021) in our study have been known to promote stem cell self-renewal and proliferation of cells including cardiomyocytes (41–43), CiCMs in an immature state right after reprogramming or cells in the middle of reprogramming might proliferate at early time points (days 3 to 7). However, we observed that cells were no longer proliferative after 14 days of chemical induction. Low numbers of proliferating Ki67^{+} cells were observed (~0.5%) in all 2D and 3D groups, and most of these proliferating cells were α-actinin negative (fig. S7, A and B). These data indicate that CiCM may proliferate at the early stage of reprogramming, but fully reprogrammed CiCMs are not proliferative anymore. The number of Ki67^{+} cells at day 14 was not significantly different between HEM and MAT groups (fig. S7B), which may indicate that cell proliferation is not significantly affected by HEM.

As embryonic fibroblasts have higher plasticity than somatic cells, we checked whether PMEFs are reprogrammed to cardiac lineage without small-molecule treatment. PMEFs cultured for 7 days on 2D MAT and 2D HEM were not positive at all for cardiac progenitor (GATA4) and cardiomyocyte markers (α-actinin and cTnT; fig. S8). This indicates that PMEF population in our study did not contain cardiomyocyte-like cells, and PMEFs were not spontaneously reprogrammed in the absence of reprogramming chemicals. We also performed cardiac reprogramming using adult fibroblasts with less developmental plasticity [tail-tip fibroblasts (TTFs)]. The same cocktail of small-molecule treatments resulted in the conversion of TTFs to beating clusters of CiCMs (fig. S9). Similar to the results from the study with PMEFs, the CiCMs reprogrammed from TTFs in 3D environment with tissue-specific ECM (3D HEM) showed the highest expression of α-actinin (fig. S9, A and B), which confirms the reproducibility of our reprogramming strategy in adult somatic cells.

3D HEM promotes cardiac maturation of CiCMs

We assessed CiCM maturation by measuring the sarcomere length in CiCMs stained with α-actinin after 14 days of chemical cardiac reprogramming (Fig. 3, A to D, and fig. S10). Immunofluorescent staining analysis for α-actinin and F-actin on day 14 confirmed that CiCMs in 3D HEM, 3D MAT, or 2D HEM, but not in 2D MAT, frequently displayed clear cross-striated patterns (Fig. 3, A and B, and fig. S10). The cells in 2D MAT showed weak and irregular signals of cross-striated pattern (Fig. 3B), whereas the cells in the other three groups showed relatively regular patterns, with those in 3D HEM exhibiting the clearest and largest cross-striated patterns (Fig. 3, B and C). The sarcomere lengths of CiCMs generated in 3D HEM or 2D HEM ranged from 1.7 to 2.0 μm (Fig. 3C), which is close to the sarcomere length of adult cardiomyocytes (44). The percentages of α-actinin^{+} cells with sarcomere structures were higher in the 2D HEM, 3D MAT, and 3D HEM cultures than in the 2D MAT cultures (Fig. 3D). The 3D HEM cultures had almost three times more cells with cross-striated sarcomere patterns compared with the 2D MAT cultures. We investigated TGF-β signaling, an important indicator of fibrotic events and a barrier to cardiac reprogramming (Fig. 3, E and F) (12, 45, 46). On day 14 of culture, phosphorylation of Smad2 (Ser[465/467]), an indicator of

TGF-β activation, was significantly reduced in the 3D HEM cultures compared with that in the 2D MAT cultures (Fig. 3, E and F).

After 21 days of culture, the cells in 3D HEM formed cTnT[+] cardiac tissue–like constructs, whereas those in 3D MAT showed clusters of cTnT[+] regions without the cardiac tissue–like morphology (Fig. 3G). The cells in 3D HEM showed highly organized α-actinin[+] sarcomeres (day 24) and were positive for cTnI with cross-striated pattern (day 21; Fig. 3H). Expression of the gap junction protein connexin 43 (Cx43) was observed in the 3D HEM cultures, whereas no such expression was observed in the 3D MAT cultures (Fig. 3I). Transmission electron microscopy (TEM) demonstrated that the CiCMs in 3D HEM displayed cardiomyogenic features, including sarcomeric structures with Z lines and myofibrils (Fig. 3J). The development of transverse tubules (t tubules) in the CiCMs of 3D HEM group was confirmed with labeling with wheat germ agglutinin (WGA; Fig. 3K). GO enrichment analysis of RNA sequencing data from the 2D MAT and 3D HEM cultures on day 21 confirmed improved cardiac conversion (Fig. 3, L and M). The 3D HEM cultures showed up-regulation of genes enriched with GO terms related to muscle contraction and cardiac muscle morphogenesis. The 3D HEM cultures also showed up-regulation of genes involved in cardiac-related molecular functions and cellular components, all consistent with a more differentiated cardiomyocyte-like state. The top 20 GO terms with the lowest P values in each group also indicated that genes involved in muscle contraction, structure, and development were up-regulated in the 3D HEM cultures compared with the 2D MAT cultures (Fig. 3M). Together, these results indicate that biochemical cues provided by both the HEM and the 3D environment are important for promoting transgene-free direct cardiac conversion.

3D HEM improves the electrical functionality of CiCMs

We next investigated spontaneous beating and calcium transients in the CiCMs by analyzing time-lapse imaging of calcium influx on day 14 of culture (Fig. 4, A to C, and movie S5 to S8). CiCMs in 3D HEM showed synchronized, spontaneous, and continuous beating, whereas CiCMs in 3D MAT, 2D HEM, or 2D MAT showed spontaneous but unsynchronized beating (movies S5 to S8). Spontaneous calcium transients were measured by Ca^{2+} imaging with Fluo-4, a fluorescently labeled calcium indicator (Fig. 4, A to C). CiCMs in 3D HEM exhibited more constant calcium influx with higher peak amplitudes, whereas CiCMs in 3D MAT, 2D HEM, or 2D MAT displayed irregular calcium transients (Fig. 4A). The cells in 3D HEM responded with synchronized beating when electrically stimulated at 1 Hz (Fig. 4B). Under 1 Hz of stimulation, the Ca^{2+} transients were paced from 0.55 ± 0.03 to 1.00 ± 0.01 s in the cells that were reprogrammed in 3D HEM, indicating that the 3D HEM CiCMs were synchronized upon electrical field stimulation (Fig. 4C).

Functional analysis of the cells reprogrammed in 3D HEM was performed on a multielectrode array (MEA) system (Fig. 4, D to I). Extracellular field potentials were monitored on 64 recording electrodes of a single well (Fig. 4, D and E). Continuous waveforms showed the contractility of the 3D HEM CiCMs (Fig. 4E). Under normal conditions, the field potential parameters of the 3D HEM CiCMs were 93.04 ± 3.63 beats per minute (BPM), 0.51 ± 0.02 mV field potential amplitude (FPA), and 143.2 ± 6.19 ms field potential duration corrected using Fridericia's rate correction algorithm (FPDcF; Fig. 4, F and G). To assess the responsiveness of
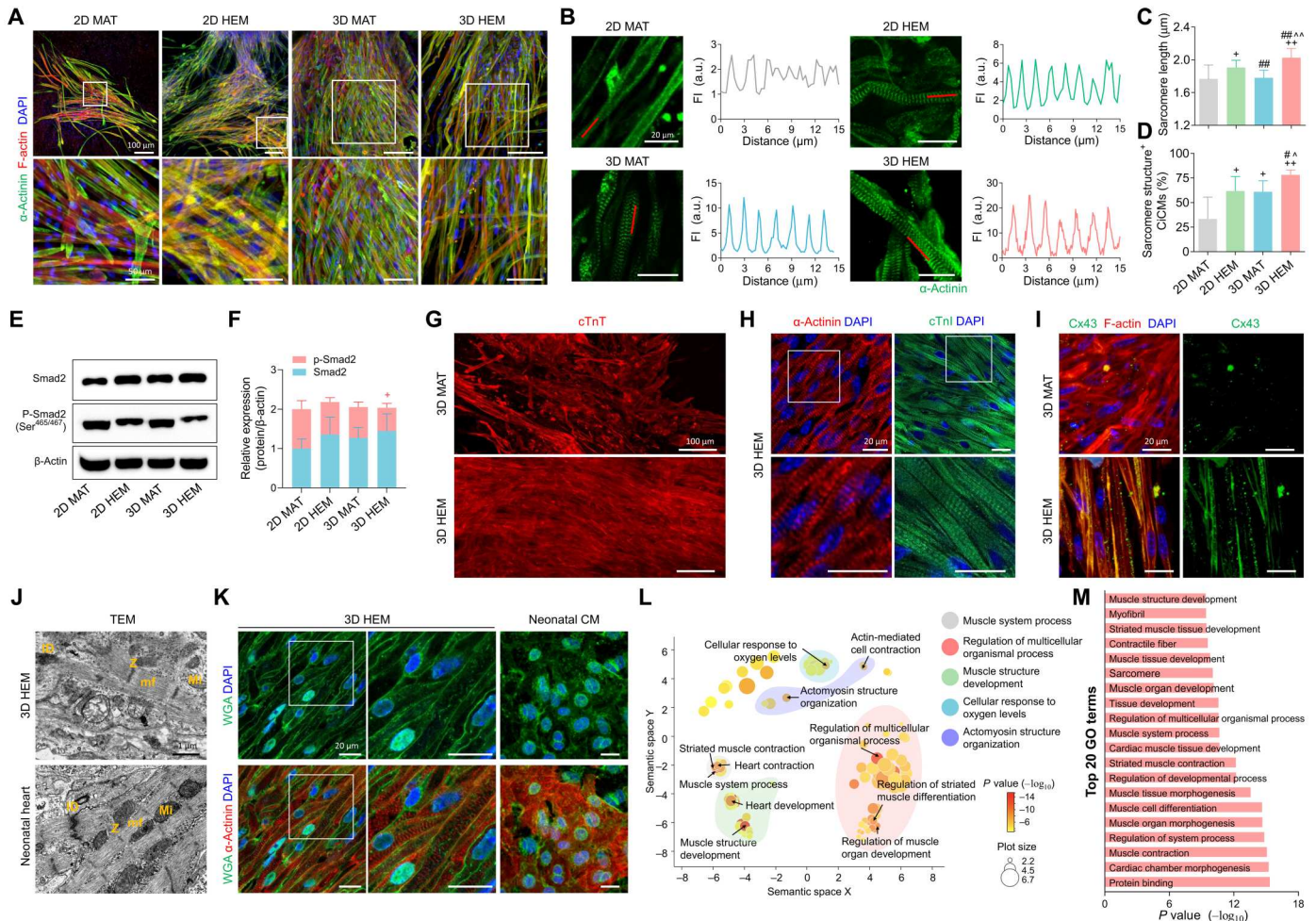
Fig. 3. Assessment of 3D HEM CiCM maturation. (**A**) Immunostaining for α-actinin in cells reprogrammed under different conditions on day 14 (scale bars, 100 μm). (**B**) Sarcomere length patterns based on fluorescence intensity (FI) changes in immunostained images for α-actinin (scale bars, 20 μm). Measurements of (**C**) sarcomere length (*n* = 12 to 20) and (**D**) sarcomere pattern–positive CiCMs (*n* = 5). (**E**) Western blot and (**F**) quantification of Smad2 and p-Smad2 expression relative to β-actin on day 14. (**G**) Immunostaining against cTnT in 3D MAT and 3D HEM CiCMs on day 21 (scale bar, 100 μm). (**H**) Immunostaining for α-actinin and cTnI in 3D HEM CiCMs on days 24 and 21, respectively (scale bars, 20 μm), and (**I**) Cx43 and F-actin in 3D MAT or 3D HEM CiCMs on day 21 (scale bars, 20 μm). (**J**) TEM images of 3D HEM CiCMs on day 21 and postnatal mouse heart (Z, Z lines; mf, myofibril; Mi, mitochondria; ID, intercalating disc) (scale bar, 1 μm). (**K**) WGA staining to confirm t-tubule formation in 3D HEM CiCMs on day 14 and neonatal CMs (scale bars, 20 μm). (**L**) GO enrichment of genes up-regulated in 3D HEM cells relative to 2D MAT cells on day 21. The scatterplot showing semantic relations among GO terms for genes up-regulated (≥2-fold) in 3D HEM cells relative to 3D MAT cells. The color indicates the *P* value, and the circle size indicates the generality of GO terms. (**M**) The top 20 most-enriched GO terms of up-regulated genes in 3D HEM cells. All data are expressed as the means ± SD. Statistical difference between the groups was determined by two-tailed *t* test (+*P* < 0.05 and ++*P* < 0.01 versus 2D MAT, #*P* < 0.05 and ##*P* < 0.01 versus 2D HEM, and ^*P* < 0.05 and ^^*P* < 0.01 versus 3D MAT). a.u., arbitrary units.

the cardiac microtissues to β-adrenergic stimulation, we treated 3D HEM CiCMs with sequentially increasing doses of isoproterenol (Fig. 4, H and I). As shown by the representative traces, treatments with 100 nM and 1 μM isoproterenol increased the BPM by 135.7 and 163.3%, respectively (Fig. 4I). These data demonstrate that CiCMs reprogrammed in 3D HEM are responsive to β-adrenergic agonist, indicating the possibility of their application for drug testing. We also performed a patch-clamp analysis to compare the electrophysiological functions between 3D HEM CiCMs and neonatal cardiomyocytes. To measure the action potentials (APs) at the single-cell level, the cells in 3D HEM were dissociated into single cells and reseeded on the HEM-coated plate. Intracellular recording of electrical activity in spontaneously beating CiCMs displayed

tracings similar to the potential observed in neonatal cardiomyocytes (Fig. 4, J and K).

HEM had tissue-specific effects on improved cardiac reprogramming

HEM can provide complex networks of heart-specific ECM that is optimal for direct cardiac reprogramming. The biochemical composition of ECM varies depending on the tissue source (*47*). Thus, the effects of ECM on cardiac conversion and maturation might be dependent on tissue type. We validated the tissue-specific effects of HEM by comparing HEM with ECMs derived from other tissues, including brain (BEM), stomach (SEM), liver (LEM), and intestine (IEM) (Fig. 5). In 2D settings, we observed a time-

Fig. 4. Electrophysiological analysis of 3D HEM CiCMs using calcium imaging and MEA. (**A**) Representative images and patterns of Ca^{2+} fluorescence visualized using Fluo-4 AM as an intracellular Ca^{2+} indicator (scale bars, 20 μm). (**B**) Calcium imaging of spontaneously beating CiCMs (top) and CiCMs electrically stimulated at 1 Hz (bottom) (scale bars, 10 μm). (**C**) Average time between Ca^{2+} transients ($n = 4$ to 7; **$P < 0.01$ versus spontaneous group, two-tailed t test). (**D** to **I**) Field potential analysis using MEA on day 16 of culture. (D) Bright-field image of a 3D HEM CiCM construct on 64 planar microelectrodes (scale bar, 200 μm) and (E) representative field potential traces from a single well. (F) A representative extracellular field potential waveform obtained from an electrode on the MEA plate. (G) Field potential parameters of 3D HEM CiCMs ($n = 8$). (H) The effect of isoproterenol on the field potentials of 3D HEM CiCMs. Representative field potential waveforms before drug (control) and in the presence of 10 to 1000 nM isoproterenol (ISO). (I) BPM change of 3D HEM CiCMs in the presence of multiple doses of isoproterenol (normalized to the control group) ($n = 3$; **$P < 0.01$ versus control group by one-way ANOVA followed by Dunnett's test). (**J**) Representative APs of the 3D HEM CiCMs after 18 days of chemical reprogramming and isolated neonatal cardiomyocyte (nCM). (**K**) Comparison of AP parameters of 3D HEM CiCMs with nCMs, including maximum diastolic potential (MDP), AP amplitude (APA), maximum upstroke velocity (dV/dt_{max}), and beating frequency (BF) ($n = 8$). All data are expressed as the means ± SD.
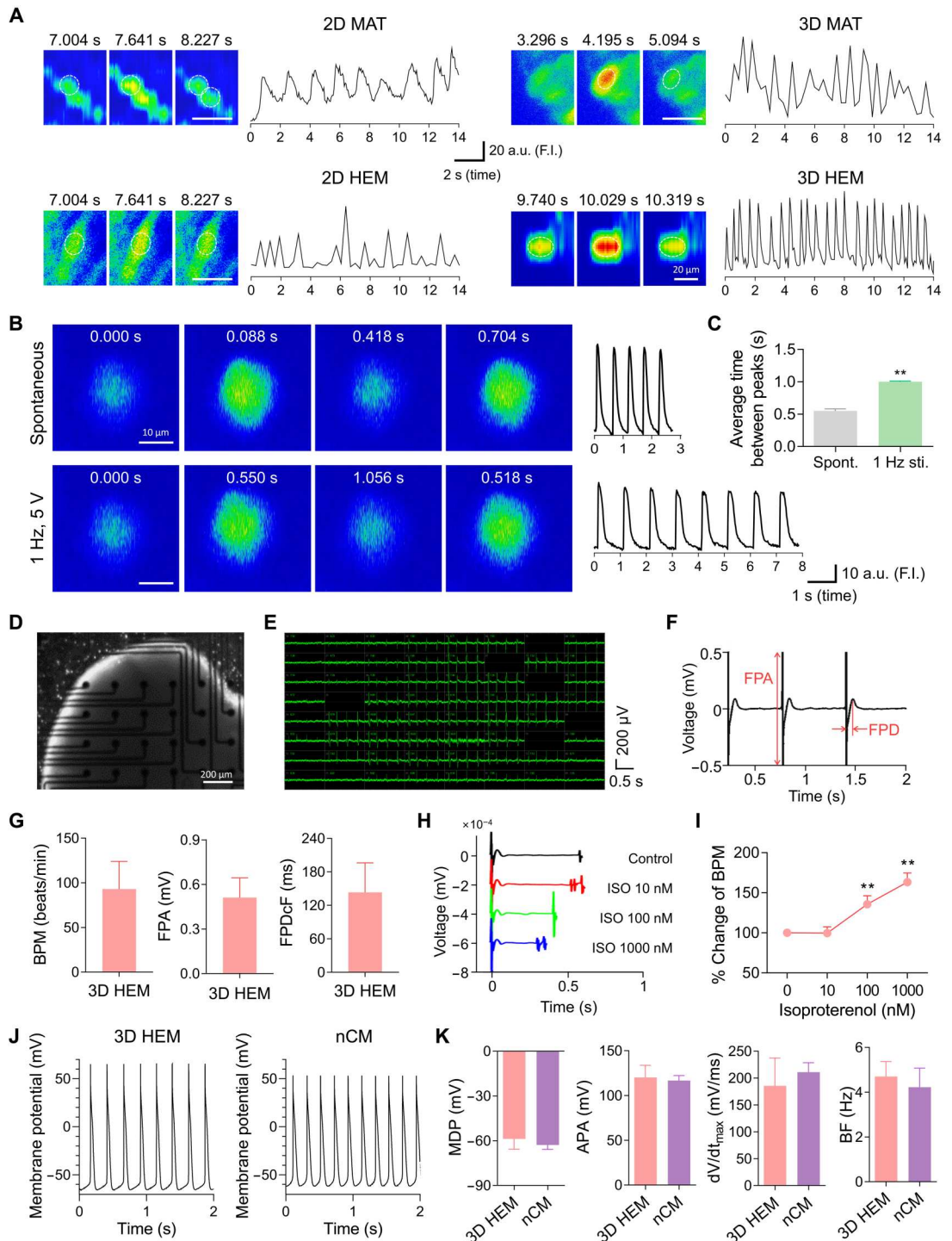
dependent increase in the number of beating clusters in all types of ECM (Fig. 5A); however, the 2D HEM contained more beating clusters than any of the other 2D ECMs. Furthermore, qPCR and immunostaining analyses showed that 2D HEM induced significantly higher levels of cardiac gene expression (*Mef2c*, *Myh7*, and *Nkx2-5*) and reprogramming to cTnT+ cells compared with other types of 2D ECM (Fig. 5, B and C). The results were similar in 3D ECM: 3D HEM appeared to be the most optimal type of 3D ECM for

chemical cardiac reprogramming (Fig. 5, D to G). Cells in 3D HEM showed higher cardiac gene expression (*Mef2c*, *Myh7*, *Nkx2-5*, *Actc1*, and *Scn5a*) and cTnT+ cell frequencies than cells in the other types of 3D ECM (Fig. 5, D and E). Although the average sarcomere length was similar among all the 3D ECMs, the sarcomeres in 3D ECMs other than 3D HEM showed irregular patterns of length (Fig. 5F). Among all the 3D ECMs, 3D HEM had the greatest numbers of CiCMs with regular sarcomere structures
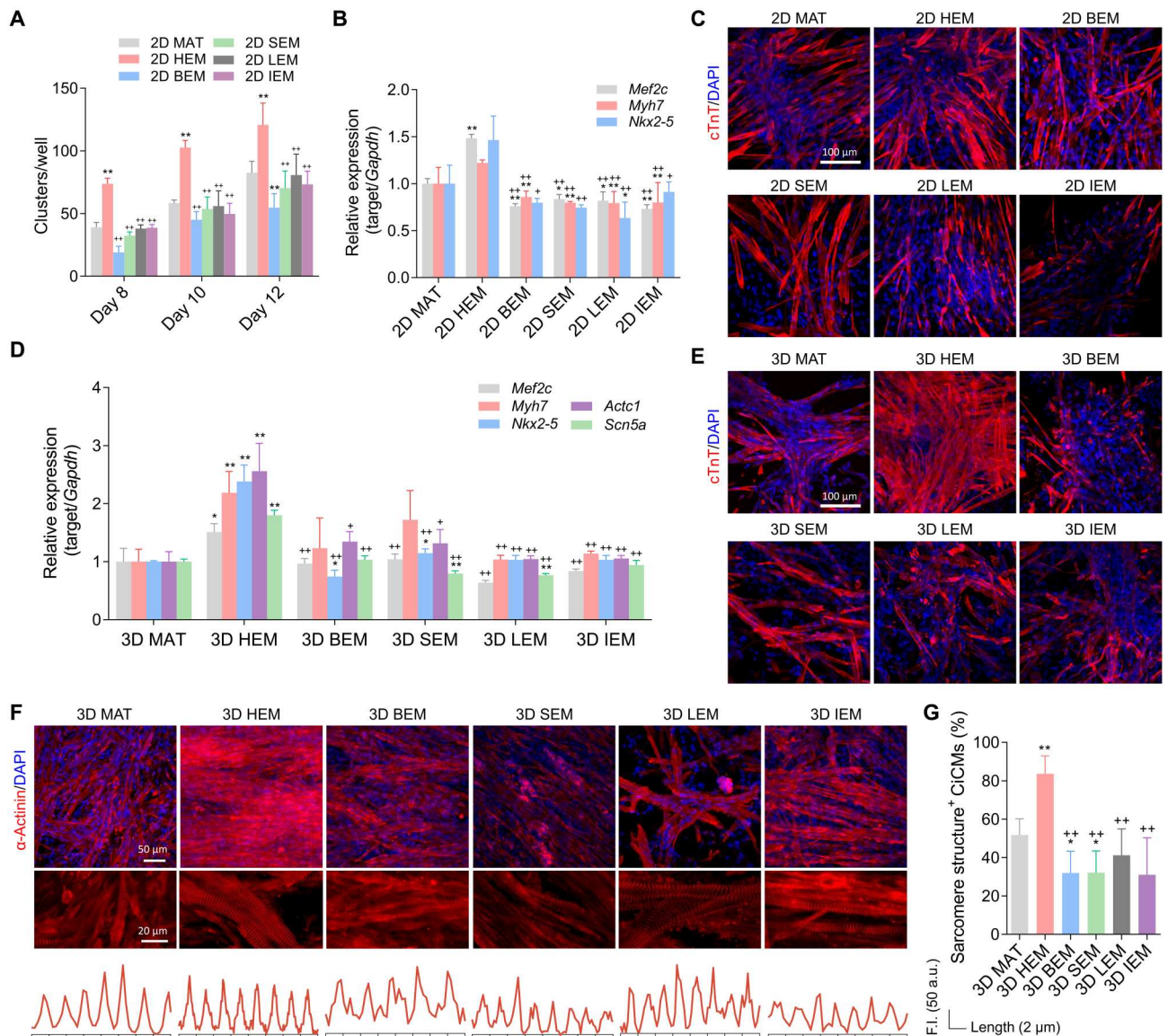
Fig. 5. Effects of various tissue-derived ECMs on direct cardiac reprogramming. (**A**) Number of beating clusters of CiCMs cultured on 2D substrates coated with various ECMs ($n = 3$). (**B**) Comparison of cardiac gene expression between various types of ECM-coated substrates by qPCR on day 14 of culture ($n = 3$). (**C**) Immunostaining for cTnT in CiCMs cultured on different tissue-derived ECM-coated 2D substrates (scale bar, 100 μm). (**D**) qPCR analysis to compare cardiac gene expression levels in CiCMs cultured in various types of 3D ECM hydrogels on day 14 of culture ($n = 3$). (**E**) Immunostaining for cTnT in CiCMs cultured in various types of 3D ECM hydrogels (scale bar, 100 μm). (**F**) Immunostaining for α-actinin in 3D-cultured CiCMs on day 14 [scale bars, 50 μm (top) and 20 μm (middle)] and analysis of sarcomere lengths (bottom). (**G**) Percentages of α-actinin+ cells that have sarcomere structures on day 14 of culture ($n = 4$ to 5). All data are expressed as the means ± SD. Statistical difference between the groups was determined by two-tailed t test (*$P < 0.05$ and **$P < 0.01$ versus MAT; +$P < 0.05$ and ++$P < 0.01$ versus HEM).

(Fig. 5, F and G). These results highlight the necessity for tissue-specific ECM in cardiac reprogramming and structural organization.

CiCMs reprogrammed in 3D HEM improved cardiac function in a rat model of MI

To explore the therapeutic potential of 3D HEM CiCMs, we induced acute MI in rats by permanently ligating the left anterior descending artery. MI occurs when blood flow to the myocardium is restricted, leading to cardiomyocyte death, adverse cardiac remodeling, and cardiac dysfunction (*48*). To check the progress of MI, we measured baseline echocardiography 1 week after inducing

MI, before injecting CiCMs. The cells harvested at 14 days of reprogramming were used for transplantation. Although reprogramming of PMEFs started from 1.25×10^4 cells per hydrogel at day 0, the number of total cells increased to 3.37 ($\pm$ 0.68) $\times 10^5$ cells per hydrogel at day 14, likely due to cell proliferation during reprogramming, and the number of α-actinin+ CiCMs at day 14 was 2.68 ($\pm$ 0.55) $\times 10^5$ cells per hydrogel. As a result, the reprogramming efficiency determined by calculating the number of CiCMs in the 3D HEM just before transplantation (14 days of reprogramming) was approximately 79.7%. We injected CiCMs reprogrammed in 2D MAT or 3D HEM at two different sites in the border zone

between the infarcted region and normal myocardium 7 days after injury, when tissue necrosis and inflammation are reduced and injured myocardium starts to be remodeled. We analyzed cardiac functions using echocardiography 1 week after MI induction (before CiCM injection) and 1 and 2 weeks after CiCM injection to investigate the engraftment of the cells (Fig. 6, A to H). Rats injected with 3D HEM CiCMs displayed improved ejection fraction (EF) and fractional shortening (FS) compared with untreated rats with MI (Fig. 6, B and C). Parameters of post-MI cardiac remodeling, such as left ventricular internal diastolic diameter (LVIDd), left ventricular internal systolic diameter (LVIDs), and relative wall thickness (RWT), indicated that adverse cardiac remodeling was partially attenuated by the injection of 3D HEM CiCMs (Fig. 6, D to F). Although there was no significant difference in posterior wall thickness (PWT) among the treatment groups, septum wall thickness (SWT) was significantly greater in rats injected with 3D HEM CiCMs than in untreated rats with MI (Fig. 6, G and H). These results indicate that treatment with CiCMs reprogrammed in 3D HEM reduced adverse cardiac remodeling and attenuated cardiac injury after MI.

CiCMs reprogrammed in 3D HEM improved hemodynamic cardiac contractibility and mitigated cardiac fibrosis in infarcted hearts

MI-induced rats injected with 3D HEM CiCMs showed significant improvement in hemodynamic cardiac function. We assessed intrinsic cardiac contractibility with pressure-volume (PV) loop to measure the hemodynamic pressure and left ventricle (LV) volume 2 weeks after transplantation (Fig. 7, A to H). The stroke volume and cardiac output, as parameters of cardiac function, were higher in rats injected with 3D HEM CiCMs than in control rats (Fig. 7, B and C). The maximum volume (V_{max}) was lowest in rats injected with 3D HEM CiCMs, indicating reduction in adverse cardiac remodeling (Fig. 7D). The maximum rate of pressure change (dP/dt_{max}) and minimum rate of pressure change (dP/dt_{min}) were higher in rats treated with 3D HEM CiCMs than in control rats, suggesting improvement in steady-state conditions of cardiac functions (Fig. 7, E and F). Because cardiac function is load dependent, we further induced temporary occlusion of the inferior vena cava (IVC) to assess the intrinsic cardiac contractibility (Fig. 7, G and H). Although the slope of the end-diastolic PV relationship (EDPVR) was comparable among all groups, the slope of the end-systolic PV relationship (ESPVR) was steeper in rats injected with
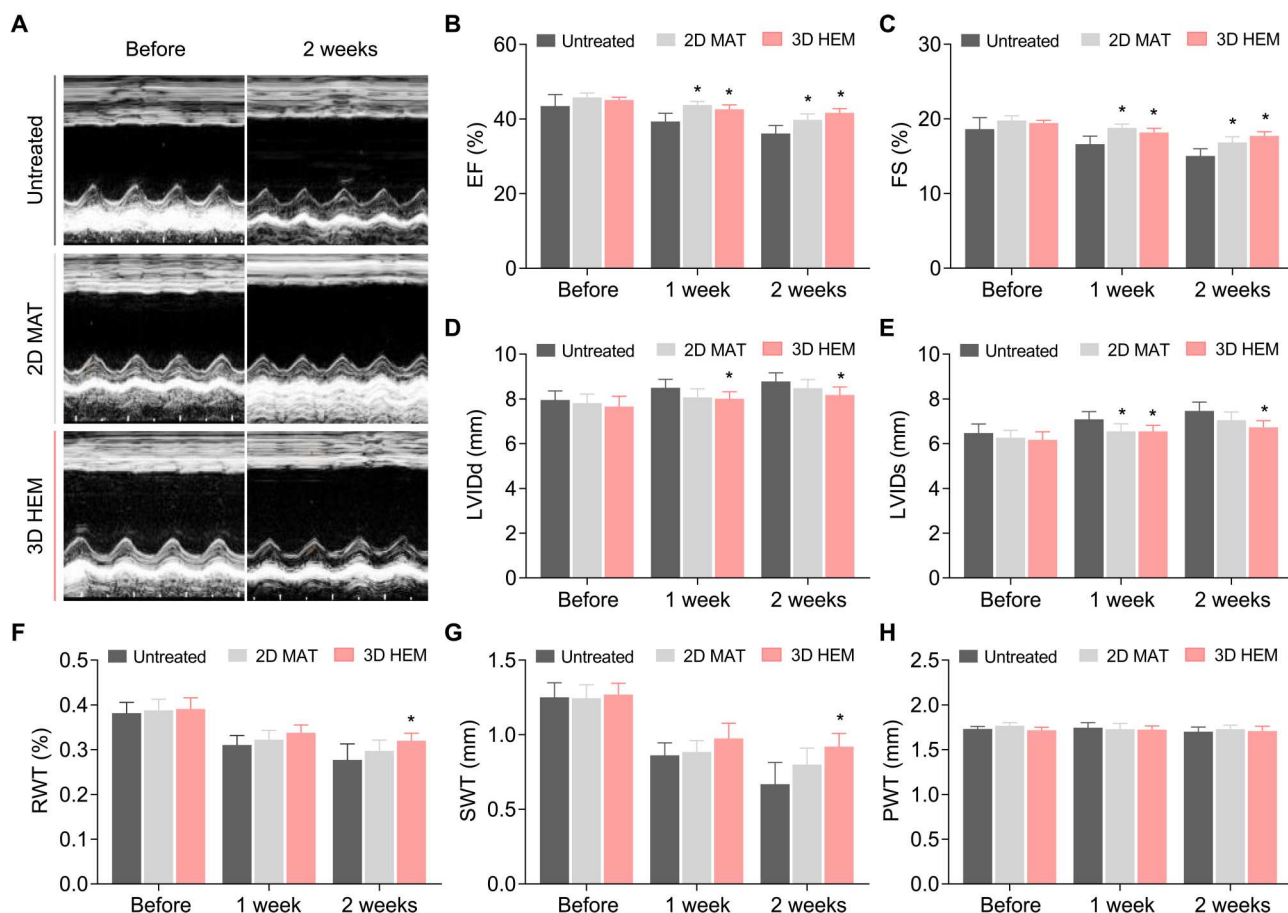

Fig. 6. Improvement of cardiac function by transplantation of 3D HEM CiCMs in a rat MI model. (**A**) Representative images of M-mode echocardiographic assessment of cardiac function in three experimental groups of MI rats (no treatment, 2D MAT CiCM, and 3D HEM CiCM) 1 week after MI (before intervention) and 1 and 2 weeks after intervention. (**B**) EF. (**C**) FS. (**D**) LVIDd. (**E**) LVIDs. (**F**) RWT. (**G**) SWT. (**H**) PWT. (B to H) All data are expressed as the means ± SD. Statistical difference between the groups was determined by two-tailed t test (n = 4 to 1, *P < 0.05 versus untreated at the same time point).
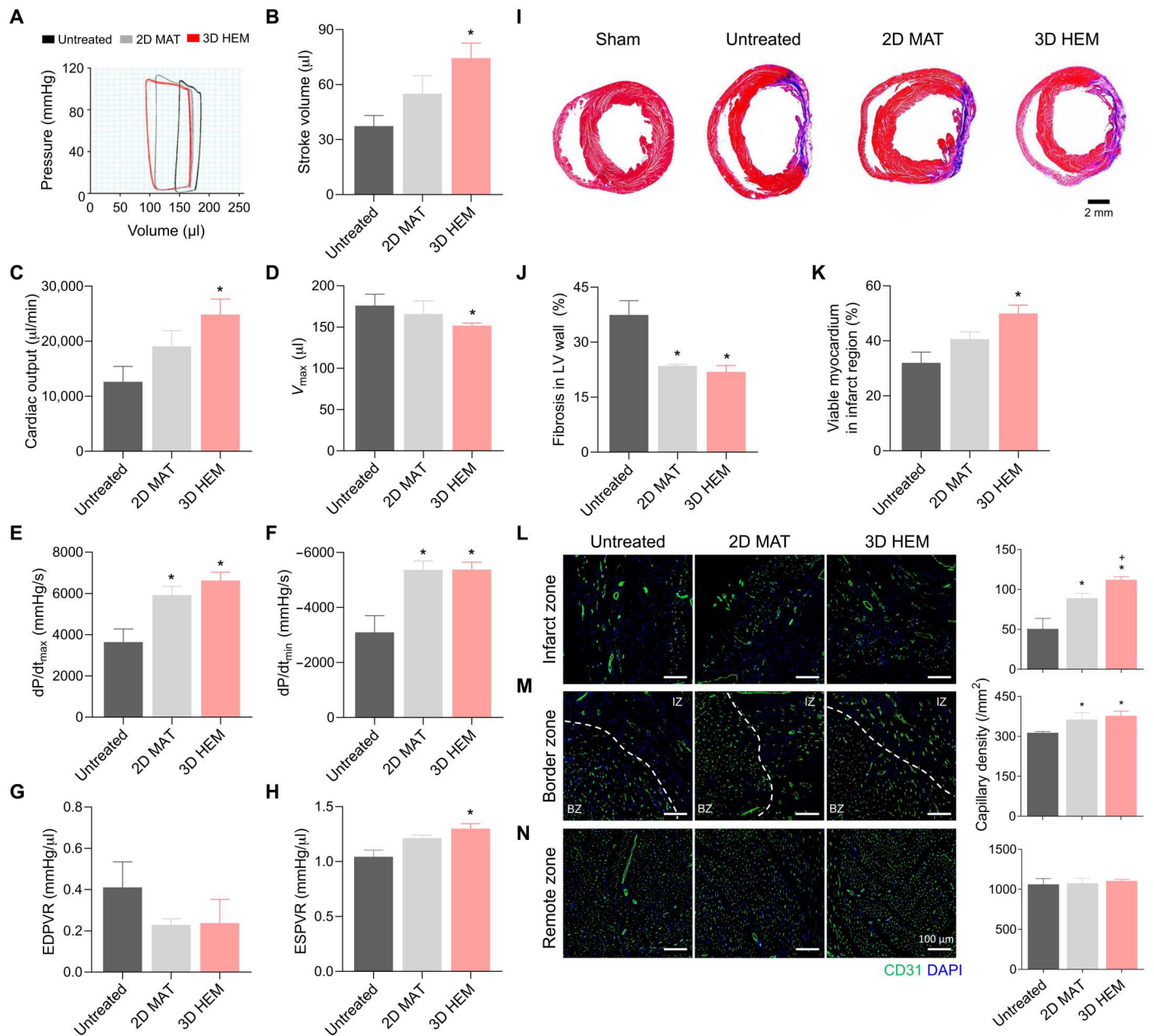
Fig. 7. Transplantation of 3D HEM CiCMs improved hemodynamic cardiac contractibility and reduced fibrosis. (**A**) Representative image of the hemodynamic pressure and volume curve at steady state 2 weeks after interventions. (**B**) Stroke volume. (**C**) Cardiac output. (**D**) Volume max (V_{max}) defining the blood volume in the LV at end diastole. (**E**) Maximal rate of pressure changes during diastole (dP/dt$_{max}$). (**F**) Minimal rate of pressure changes during diastole (dP/dt$_{min}$). (**G**) Slope of the EDPVR. (**H**) Slope of the ESPVR. (**I**) Representative images of MT staining using the heart tissues harvested 2 weeks after interventions (scale bar, 2 mm). Sham control without ischemia induction served as a native heart tissue. Percentages of (**J**) fibrotic area in the LV and (**K**) viable myocardium in the infarcted region based on MT-stained images. (**L** to **N**) Representative images of capillaries stained with CD31 (green) on the infarct zone, border zone, and remote zone 2 weeks after interventions (scale bars, 100 μm). Statistical difference between groups was determined by two-tailed *t* test (*n* = 3 to 5; *P < 0.05 versus untreated; +P < 0.05 versus 2D MAT).

3D HEM CiCMs than in the other groups (Fig. 7, G and H). Collectively, these findings suggest that transplantation of CiCMs reprogrammed in 3D HEM improves cardiac repair in MI hearts.

To investigate the therapeutic effects of 3D HEM CiCMs on cardiac fibrosis, we quantified fibrosis in the infarcted regions of rat hearts using MT staining 2 weeks after CiCM transplantation (Fig. 7, I to K). MT staining demonstrated that treatment with 3D

HEM CiCMs significantly reduced the fibrotic area in the LV wall and increased the amount of viable myocardium in the infarcted region. Subsequently, we assessed neovascularization by immunohistochemical staining of CD31+ capillaries. The CD31+ capillary density in the border and infarcted zones of ischemic hearts was highest in rats treated with 3D HEM CiCMs (Fig. 7, L and M), whereas the capillary densities in remote zones were similar

between all groups (Fig. 7N). Since the therapeutic effects of cell-based therapy depend on the engraftment of transplanted cells, we investigated the engraftment of transplanted CiCMs fluorescently labeled with 1,1′-dioctadecyl-3,3,3′,3′-tetramethylindocarbocyanine perchlorate (DiI) 2 weeks after transplantation (fig. S11A). We observed more efficient engraftment of the 3D HEM CiCMs, as indicated by the larger number of DiI- and cTnT-copositive cells in the 3D HEM group than in the 2D MAT group (fig. S11, A and B). Although CiCMs with a more mature morphology were occasionally observed in the 3D HEM group compared to the 2D MAT group, CiCMs interacting with host cardiomyocytes were rarely detected at this time point (~2 weeks). Overall, our results demonstrate that CiCMs reprogrammed in 3D HEM ameliorate infertile microenvironments and show improved engraftment capacity in the infarcted heart, as indicated by reduced cardiac fibrosis and enhanced neovascularization and retention of CiCMs.

DISCUSSION

Despite recent progress in direct cardiac reprogramming, further improvement in reprogramming efficiency and maturation is necessary. Shortening the time required to prepare functional cardiomyocytes via direct cardiac reprogramming will be vital for successful treatment of patients who suffer from MI at an acute or subacute stage. Several previous studies reported the positive effects of 3D settings (e.g., fibrin and MAT) on cardiac reprogramming of fibroblasts (22, 49). However, those studies used genetic manipulation for reprogramming (transfection with a set of microRNAs), which may evoke potential safety issues, and also did not examine the tissue-specific effects of ECM environment to boost lineage specification during reprogramming. Here, we further highlighted the critical roles of tissue-specific ECM cues in the reprogramming process without genetic alteration.

Our results demonstrate that a cardiac-specific 3D extracellular microenvironment promotes chemically induced direct reprogramming of fibroblasts into functional cardiomyocytes. HEM is composed of structural and matricellular components and soluble factors that provide structural support and direct cells to differentiate into the cardiac lineage. The use of 3D HEM generated spontaneously beating cells with structural maturation, improved contractility, and synchronization at a higher rate than the use of 3D MAT or 2D substrates. HEM contained several ECM proteins that are known to be essential in cardiac development, such as collagens (I, IV, V, and VI), heparin sulfate proteoglycan, versican, fibrillin-1 and fibrillin-2, and fibronectin (32, 50, 51). Several proteins contained only in HEM, which were absent in MAT, were found to be involved in heart development and muscle structure development (Fig. 1J). Accordingly, CiCMs reprogrammed in 3D HEM exhibited improved regenerative capability compared with those reprogrammed in other substrates in an MI model. To the best of our knowledge, ours is the first study to investigate the therapeutic potential of CiCMs directly reprogrammed in heart-derived 3D ECM. 3D HEM format can synergistically improve the chemical cardiac reprogramming and regenerative potential of the induced cardiomyocytes owing to the combined effect of biochemical cues (heart-enriched ECM components) and biophysical cues (3D soft environment).

3D HEM culture seems to be more favorable for cardiac reprogramming and maturation than 2D culture. 3D culture system owns different chemical and mechanical properties with respect to the 2D culture system. Cells cultured in 3D hydrogels show different cell-cell and cell-matrix interactions that direct various biological processes to induce stem cell specification and differentiation. For example, a previous study reported significantly higher expression of matrix metalloproteinases in 3D-cultured fibroblasts than in 2D-cultured cells during direct reprogramming via a combination of microRNAs (22). This might precondition fibroblasts to be more amenable to be converted into cardiomyocyte-like cells. The local mechanical forces via cell-matrix and cell-cell adhesion also lead to epigenetic regulation through changes in the chromatin structure and arrangement (52–54). The mechanical force from the ECM is transmitted to the nucleus through the cytoskeleton via the linker of nucleoskeleton to cytoskeleton complex, which modulates chromatin organization and gene transcription. Previous studies investigated how mechanical cues regulate cell behaviors in 2D substrates and 3D matrices (55–59). The mechanical cues exerted by different ECM stiffnesses in 2D and 3D conditions alter biochemical signals through focal adhesion (e.g., integrins and focal adhesion kinase) and mechanosensors (e.g., YAP and talin) and ultimately affect nuclear signaling factors that modulate chromatin modification and subsequent gene expression. For example, softer matrices exerted a lower traction force to cells, resulting in a lower level of chromatin compaction in the nucleus (60). In addition, unlike 2D substrates, cell spreading, migration, and growth are confined within 3D matrices, leading to different levels of cell-ECM and cell-cell interactions. In our previous study, direct neuronal reprogramming was enhanced in 3D ECM settings compared to the 2D ECM, suggesting that soft 3D matrix could induce changes in chromatin structures to lower the epigenetic barriers of direct reprogramming (e.g., H3K4me3 and H3K27ac) (19). Thus, 3D HEM may also recapitulate the HEM-enriched microenvironment to activate mechanosensitive signals for cardiac differentiation via regulation of mechanotransducer activity (e.g., YAP) (19). Overall, biophysical and mechanosensitive modulation of 3D HEM may induce regulatory signaling changes favorable for enhancing conversion efficiency and cardiac maturation.

Viscoelasticity of culture matrix is emerging as an important determinant of cell behavior and fate regulation (61–63). A previous report demonstrated that when mesenchymal stem cells were cultured on functionalized alginate hydrogels with the same initial elastic modulus but different stress relaxation times, they displayed different levels of osteogenic differentiation (61). Another study showed that the 3D-functionalized hyaluronic acid hydrogel containing dynamic cross-links with varied kinetic constants induced different cell-hydrogel interactions and stem cell behaviors (62). The hydrogel with fast binding kinetics and short binding lifetime increased the spreading of mesenchymal stem cells. In addition, the conjugation of cell-adhesive ligands to the hydrogel subnetwork with fast binding kinetics enhanced cell spreading and mechanosensing, ultimately promoting osteogenic differentiation. By contrast, conjugation of the cell-adhesive motifs to the hydrogel subnetwork with slow binding kinetics promoted adipogenesis, although this hydrogel system had the same mechanical properties and level of network dynamics as the system with fast binding kinetics. These results highlight the importance of both chemical and mechanical forces for regulating stem cell fate.

In our study, the concerted action of tissue-specific biochemical signals, cell-intrinsic forces exerted on the ECM, and cell-ECM

interactions may guide cardiac reprogramming. As the biochemical composition of the ECM largely determines the specificity of integrin binding and subsequent cell responses (64), HEM could provide more optimal integrin-ECM interactions for cardiac lineage specification compared to other ECMs. In addition to its chemical composition, the viscoelasticity of 3D HEM hydrogel would also be an important regulator of cell reprogramming because cells respond to ECM elasticity via integrins and actomyosin-driven traction forces, which affects focal adhesion assembly, cytoskeletal organization, and signal transduction (65, 66). Dimensionality of the 3D matrix may also affect cell-ECM interactions. 3D HEM contains the same ECM compositions as 2D HEM coated on the substrates, but cells in 3D HEM are likely to exhibit different adhesion dynamics from cells in 2D HEM. For example, a previous study demonstrated that the adhesion composition and localization associated with fibronectin-based fibrils in 3D matrix differed from the adhesion formation on 2D fibronectin (67). The content of $\alpha5\beta1$ integrins, paxillin, and level of tyrosine phosphorylation of focal adhesion kinase were different between 2D and 3D conditions. Although the adhesion kinetics in 3D ECM is far more complex and is affected by other factors such as porosity and fiber alignment, it was suggested that 3D matrices could induce longer adhesion longevity and faster adhesion protein kinetics, as displayed by increased integrin-ECM adhesion binding and dissociation rates (68). Overall, the interplay of biochemical ECM components, viscoelasticity, and dimensionality of 3D HEM hydrogel seems to reconstitute microenvironments favorable for cardiac direct reprogramming.

Although heart-mimetic biochemical ECM cues provided in a 3D format led to increased cardiac conversion efficiency and more mature phenotypes, the maturity of CiCMs still needs to be improved to meet the maturity level of adult cardiomyocytes. CiCMs look less mature than neonatal cardiomyocytes containing aligned myofibrils with well-organized Z lines and densely packed and aligned mitochondria (Fig. 3J). Although the CiCMs reprogrammed in 3D HEM exhibited some of the hallmarks of mature cardiomyocytes, including the expression of myofilament proteins and sarcomeres, the sarcomeres were less organized compared to those in the neonatal heart. Thus, CiCMs need to be further structurally matured to the levels of native cardiomyocytes. We observed DiI-positive CiCMs showing clear sarcomeric patterns in the transplanted region, but these populations of cells were rarely found (fig. S11A). One possibility for this observation is that harsh microenvironments (e.g., hypoxia and inflammation) in the infarcted site with ischemic injury might affect the phenotypes of CiCMs. As reprogrammed cells are known to be vulnerable to external microenvironmental changes due to epigenetic memory and instability (69), phenotypic maintenance of reprogrammed cells is likely to be more complicated especially under in vivo conditions. In addition, since we did not use biomaterial scaffolds for CiCM transplantation, retention of CiCMs exhibiting mature phenotypes might be reduced in the infarcted region. To support the phenotypic maintenance and survival of transplanted CiCMs better, functional hydrogels that can alleviate adverse effects resulting from ischemic damage and improve the survival of CiCMs would be considered for the administration of CiCMs into ischemic myocardium. Further studies are needed to uncover the mechanisms of 3D HEM effects on CiCM maturation in vitro and the long-term regenerative capability of CiCMs in vivo. The integration of the engrafted CiCMs with the host cardiomyocytes should be examined at longer time points to justify the improvement of in vivo cardiac function by the engrafted CiCMs. Because developing cardiac cells in vivo are exposed to the combined effects of diverse soluble factors and mechanical and electrical cues, it is likely that a combination approach can lead to greater CiCM functionality and therapeutic efficacy in vivo. For example, electric fields that mimic the bioelectrical environment of the native heart might further enhance the maturation of CiCMs (21). Thus, chemical cardiac reprogramming might be further improved by fabricating HEM hydrogels with electroconductive materials.

Actually, some products based on decellularized tissue ECM have been approved by the Food and Drug Administration for clinical application (70), while MAT derived from mouse sarcoma, a commonly used ECM for cardiac reprogramming, is not allowed to be used for humans. Therefore, chemical reprogramming without genetic alteration in 3D HEM hydrogel can make a significant contribution to the production of clinically applicable cardiac cells or tissues for therapeutic applications, which indicates an advancement in reprogramming technology by our strategy used in this study. Nevertheless, clinical application of decellularized tissue–derived ECM may be limited because of its chemically undefined composition. As a future direction, proteomic-based screening for key ECM determinants in HEM that drive cardiac reprogramming and maturation could be considered to explore chemically defined alternatives to decellularized tissue matrices (71). Furthermore, a 3D matrix with additional adhesive property that is strong enough to keep intact on a continuously beating heart would also be desirable. Tissue-adhesive ECM hydrogels can be prepared via biomimetic modification of adhesive moieties to polymer backbone (72). In this way, CiCMs could be directly transplanted together with the adhesive 3D matrix for MI treatment, thereby improving the therapeutic efficacy of transplanted CiCMs (73, 74).

MATERIALS AND METHODS
Heart tissue decellularization
LVs were isolated from whole porcine hearts obtained from a local market. Heart tissue decellularization was performed as described previously with some modifications (75). In brief, fat tissues and blood clots were removed, and the LV tissues were cut into small pieces (≈2 mm by 2 mm by 2 mm). The pieces were decellularized by serial treatment with 1% (w/v) SDS (Sigma-Aldrich, St. Louis, MO, USA) for 24 hours and then with 1% (w/v) Triton X-100 (Sigma-Aldrich) with 0.1% (v/v) ammonium hydroxide (Sigma-Aldrich) for 6 hours at 4°C with agitation at 180 rpm. The decellularized tissues were then rinsed with distilled water for 24 hours, sterilized with 1% (v/v) penicillin-streptomycin (Thermo Fisher Scientific, Waltham, MA, USA) for 2 hours, and rinsed with distilled water again. The sterilized tissues were lyophilized and stored at 4°C until use.

Decellularization assessments
For histological assessments, native and decellularized heart tissues were embedded in paraffin and sectioned at 4 μm thickness. For confirmation of successful cell removal, the sections were stained with hematoxylin and eosin. For quantification of DNA, the lyophilized native and decellularized heart tissues were homogenized with proteinase K solution in a genomic DNA extraction kit

(#9765A, TaKaRa Bio Inc., Kusatsu, Shiga, Japan) at 56°C for 3 hours, and DNA was extracted according to the manufacturer's protocol. The extracted DNA was then fluorescently stained using a Quant-iT PicoGreen dsDNA assay kit (#P11496, Thermo Fisher Scientific), and fluorescein intensities (excitation, 480 nm and emission, 520 nm) were measured to calculate the content of cellular DNA in tissues. ECM contents retained in decellularized tissues were validated by MT and Alcian blue staining for collagen and GAG, respectively. For collagen quantification, collagen was extracted from tissues using a collagen isolation and concentration protocol (76). In brief, tissues were digested in 1 ml of 0.02 M HCl (Sigma-Aldrich) solution with 4 mg of pepsin (#P7000, Sigma-Aldrich). Reagents in a Sircol soluble collagen assay (Biocolor Ltd., Carrickfergus, UK) were added to the samples for collagen concentration, and then collagen precipitates were washed, and the rest of the assay was performed following the manufacturer's instructions. For GAG quantification, tissues were digested in papain solution (#P4762, Sigma-Aldrich) at 60°C overnight. The GAG contents in digested solutions were stained with 1,9-dimethyl methylene blue (#341088, Sigma-Aldrich) and quantified using chondroitin sulfate A (#C9819, Sigma-Aldrich) as a standard. The DNA, collagen, and GAG yields were quantified spectrophotometrically using a microplate reader/spectrophotometer (Infinite M200 Pro, Tecan, Maennedorf, Switzerland).

Protein sample preparation for MS analysis
Proteins in each sample were digested using a filter-aided sample preparation protein digestion kit (Abcam, Cambridge, UK). In brief, the proteins in lyophilized tissues were reduced with 0.1 M dithiothreitol (Sigma-Aldrich) and 50 mM ammonium bicarbonate (Abcam) at 60°C for 30 min. The samples were then processed for cysteine alkylation by treatment with 100 μl of 500 mM iodoacetamide (Abcam) in 8 M urea (Abcam) for 30 min at room temperature in the dark. Trypsin (Sigma-Aldrich) was added at an enzyme-to-protein ratio of 1:50, and the proteins were digested at 37°C overnight. The supernatant of the digested samples was diluted and used for subsequent protein purification.

LC-MS/MS analysis
Liquid chromatography with tandem MS (LC-MS/MS) analysis was performed as previously reported (77). Each peptide sample was desalted with a C18 spin column (Thermo Fisher Scientific). The samples were resuspended in water/acetonitrile (ACN; Thermo Fisher Scientific) (98:2, v/v) containing 0.1% formic acid (FA; Sigma-Aldrich) and analyzed using a Q Exactive mass spectrometer coupled with an EASY-nLC 3000 system (Thermo Fisher Scientific). The peptides were separated on a two-column setup with a trap column (100 μm by 2 cm, nanoViper C18, 5 μm, 100 Å Acclaim PepMap 100, Thermo Fisher Scientific) and an analytic column (75 μm inside diameter × 50 cm long, 2-μm C18 beads, spherical fully porous ultrapure, Thermo Fisher Scientific). Solvents A and B were water/ACN (98:2, v/v) with 0.1% FA and 0.1% FA in ACN, respectively. A 180-min linear gradient from 10 to 40% solvent B was used for global profiling. The spray voltage was 2.2 kV in positive ion mode, and the temperature of the heated capillary was set to 300°C. Mass spectra were acquired in a data-dependent manner using a top 10 method on a Q Exactive. Xcaliber software version 3.1 (Thermo Fisher Scientific) was used to collect MS data. Full MS data were acquired in a scanning range of 350 to 1800 mass/

charge ratio (m/z) at a resolution of 70,000 at m/z 200 with an automated gain control target value of 3.0×10^6. The isolation window for MS/MS was 2.0 m/z. Higher-energy collisional dissociation scans were acquired at a resolution of 17,500 and 27 normalized collision energy. The automatic gain control target value for MS/MS was 1×10^5. The maximum ion injection time for survey scan and MS/MS scan was 100 ms. The dynamic exclusion time was set to 15 s. Mass data were acquired automatically using Proteome Discoverer 2.4 (Thermo Fisher Scientific).

Proteomic analysis of HEM
Proteomic analysis was performed on a total of 6 samples of MAT (n = 3) and HEM (n = 3) as previously described (75). Briefly, protein identification and label-free quantification were performed using MaxQuant (version 1.6.2.3), and proteins were identified by searching MS and MS/MS data of peptides against the *Mus musculus* UniProt database (August 2020 released) for MAT and against the *Sus scrofa* UniProt database (August 2020 released) for HEM using the Andromeda search engine (78). As acceptance criteria of the protein hit, up to two missed cleavages were allowed. Carbamidomethylation of cysteines was set as a fixed modification. Oxidation of methionine and N-terminal acetylation were set as dynamic modifications. Proteins and peptides were filtered for a false discovery rate less than 1% for significance. The iBAQ algorithm (79), which is integrated into the MaxQuant software, was used to determine the abundance of a protein by dividing the intensity value by the number of theoretical peptides of the protein. The iBAQ values were used for quantitative data analysis. The categorization of the proteins identified in MAT and HEM was done according to the public database provided by the Matrisome Project (80) and the Human Protein Atlas (81). GOBP analysis was performed using Protein Analysis Through Evolutionary Relationships (82). Visualization of nonredundant GOBP term enrichment was carried out with REVIGO (http://revigo.irb.hr).

HEM hydrogel formation
HEM was prepared by solubilizing 10 mg of decellularized heart tissue per 1 ml of 0.02 M HCl (Sigma-Aldrich) solution with 4 mg of pepsin (#P7125, Sigma-Aldrich) and stirring at 240 rpm at room temperature for 48 hours. The HEM solution was then mixed with 10× phosphate-buffered saline (PBS; Sigma-Aldrich) and diluted with distilled water to a final concentration of 5 mg/ml. Last, the pH of the mixture was neutralized by adding 0.5 M sodium hydroxide (NaOH, Sigma-Aldrich). Pepsin from porcine gastric mucosa used in our study (#P7125, Sigma-Aldrich) is known to have an optimal activity at pH 2 to 4 and become irreversibly inactive as the pH increases to 8.0 to 8.5 according to the manufacturer's instruction. Thus, the activity of pepsin in 3D HEM hydrogel neutralized with NaOH should be negligible. There were no purification steps to eliminate pepsin or the salts of HCl and NaOH in the pregel solution.

Rheological analysis of 3D hydrogels
The viscoelastic moduli of MAT and HEM hydrogels with CiCMs cultured for 1 or 5 days or without cells were measured using a rotating rheometer (MCR 102, Anton Paar, Ashland, VA, USA). The storage modulus and loss modulus of the samples were measured in a frequency sweep mode ranging from 0.1 to 10 Hz at a constant strain (1%). The average storage modulus at 1 Hz was determined

as the elastic modulus. A measuring plate with a diameter of 8 mm was used to press the hydrogels.

Cell culture

PMEFs were isolated from day 12.5 to 13.5 embryos of Institute of Cancer Research (ICR) mice (Orientbio, Seongnam, Korea), as previously reported (19). Adult TTFs were isolated from a female ICR mouse (6 to 7 weeks old; Orientbio). Isolated fibroblasts were seeded on a 0.2% (w/v) gelatin (Sigma-Aldrich)–coated flask in Dulbecco's modified Eagle's medium (DMEM; Thermo Fisher Scientific) supplemented with 10% (v/v) fetal bovine serum (FBS; Thermo Fisher Scientific) and 1% (v/v) penicillin-streptomycin (Thermo Fisher Scientific). PMEFs were cultured in 5% CO_2 at 37°C, and the medium was exchanged every 2 days. Mouse neonatal cardiomyocytes were isolated from the hearts of 2-day-old C57BL/6J mice (Orientbio). Ventricular tissue was incubated with 0.1% trypsin solution (Welgene, Gyeongsan, Korea) in Hanks' balanced salt solution (HBSS; Welgene) with gentle agitation at 4°C overnight. On the next day, the digested tissue was transferred to a petri dish on ice, minced, and collected into a conical tube. Digestion solution, comprising collagenase B (1 mg/ml; Roche, Basel, Switzerland) in HBSS, was added to the heart tissue and triturated multiple times and incubated in a 37°C water bath for 5 min with gentle agitation. The supernatant containing cardiomyocytes was transferred to isolation medium [DMEM containing 20% FBS (Thermo Fisher Scientific) with 1× antibiotic-antimycotic (Thermo Fisher Scientific)], and the undigested heart tissue was resuspended in digestion solution. An additional digestion step was performed, and the cell-containing supernatant was collected. The digestion step was repeated five times, followed by centrifugation for 10 min at 1500 rpm and washing the cell pellet in isolation medium, followed by centrifugation for 5 min at 1500 rpm and resuspension of the cell pellet in Dulbecco's PBS for use in Percoll (#17-5445-02, GE Healthcare, Chicago, IL, USA) density-gradient centrifugation. Contamination of fibroblasts and endothelial cells was removed by Percoll density-gradient centrifugation for 30 min at 3000 rpm at 4°C. Next, the cardiomyocytes were transferred to a new conical tube and resuspended in isolation medium, followed by centrifugation for 10 min at 1500 rpm and washing of the cell pellet in isolation medium. Additional centrifugation for 5 min at 1500 rpm and resuspension of the cell pellet in isolation medium were performed. The cells were plated on 0.1% (w/v) gelatin (Welgene)–coated culture plates at a density of 1×10^5 cells/cm^2. FBS was excluded to suppress the growth of noncardiomyocytes, and the medium contained 5% horse serum (#H1138, Sigma-Aldrich) and 1× antibiotic-antimycotic (Thermo Fisher Scientific). The culture medium was exchanged every other day. Primary isolation of PMEFs and neonatal cardiomyocytes was approved by the Institutional Animal Care and Use Committee (IACUC) of Yonsei University (IACUC-A-201702-131-01) and the IACUC of Yonsei University Health System (2021-0257).

Generation of CiCMs

For 2D cardiac reprogramming, HEM and other tissue-derived ECMs were coated on well plates at 0.05 mg/ml diluted in 0.2 M acetic acid (Sigma-Aldrich) for 2 to 3 hours at 37°C. As a control, MAT (Corning Incorporated, Corning, NY, USA) diluted 1:50 (v/v) in DMEM/nutrient mixture F-12 (DMEM/F12, Thermo Fisher Scientific) was coated for 1 to 2 hours at 37°C. For 3D cardiac

reprogramming, 3D HEM and other tissue-derived ECM hydrogels (SEM, IEM, and LEM) were constructed at a concentration of 5 mg/ml, as previously reported (83). BEM hydrogel was prepared as previously described (19). PMEFs were seeded on plates at a density of 2.5×10^4 cells/ml for 2D cardiac reprogramming or encapsulated in hydrogels at a density of 2.5×10^5 cells/ml for 3D cardiac reprogramming. The ECM pregel solution (50 µl) containing cells (1.25×10^4 cells per hydrogel construct) was dispensed onto the hydrophobic parafilm surface and incubated at 37°C for 30 min. The resultant ECM hydrogel formed a dome-shaped construct. After 4 hours of cell seeding or encapsulation, the PMEF culture medium was replaced with cardiac reprogramming-induction medium consisting of DMEM/F12, 15% FBS (Thermo Fisher Scientific), 5% knockout serum replacement (Thermo Fisher Scientific), 1% (v/v) penicillin-streptomycin (Thermo Fisher Scientific), 1% (v/v) nonessential amino acids (Thermo Fisher Scientific), 1% (v/v) GlutaMAX (Thermo Fisher Scientific), 0.1 mM β-mercaptoethanol (Thermo Fisher Scientific), and the following small molecules: 10 µM CHIR99021 (LC Laboratory, Woburn, MA, USA), 2 µM A83-01 (Tocris Bioscience, Bristol, UK), 15 µM Forskolin (LC Laboratory), and 1 µM SC-1 (Cayman Chemical, Ann Arbor, MI, USA) (21, 84). For reprogramming TTFs, 3 µM rolipram (Tocris Bioscience) was added in addition to the small molecules stated above. After 14 days of culture, cells were cultured in the maintaining media consisting of DMEM/F12 medium with 15% FBS, 2 µM CHIR99021, leukemia inhibitory factor (1000 U/ml), vitamin C (50 µg/ml; Sigma-Aldrich), and insulin (1 µg/ml; Sigma-Aldrich).

Immunocytochemical staining

Cells in 2D and 3D samples were fixed using 10% (v/v) formalin solution (Sigma-Aldrich) for 10 or 40 min, respectively. For cryosectioning 3D samples, the constructs were incubated in a 30% (v/v) sucrose (Sigma-Aldrich) solution in PBS overnight at 4°C. The samples were then embedded in optimal cutting temperature (OCT) compound (CellPath, Newtown, UK), frozen at −80°C, and then sliced into 10-µm sections for fluorescence imaging. The 2D samples and sectioned 3D samples were permeabilized by 0.1% Triton X-100 (Sigma-Aldrich) for 10 min, and the 3D samples for whole mounting were treated with 0.2% Triton X-100 for 20 min. After blocking with 4% bovine serum albumin (Fraction V, MP Biomedicals, Asse-Relegem, Belgium) and 2% horse serum (Thermo Fisher Scientific) for 1 hour (2D samples and sectioned 3D samples) or 2 hours (3D samples for whole mounting), the cells were incubated with primary antibodies at 4°C overnight. The antibodies used in this study were mouse monoclonal anti–α-actinin (1:500; #A7811, Sigma-Aldrich), mouse monoclonal anti-cTnT (1:200; #MA5-12960, Thermo Fisher Scientific), and rabbit polyclonal Cx43 (1:300; #C6219, Sigma-Aldrich). After thorough washing with PBS, secondary antibodies conjugated with anti-mouse Alexa Fluor 488 (1:200; #A11001, Thermo Fisher Scientific), anti-mouse Alexa Fluor 594 (1:200; #A11005, Thermo Fisher Scientific), or anti-rabbit Alexa Fluor 594 (1:200; #A11012, Thermo Fisher Scientific) were used. Tetramethyl rhodamine isothiocyanate–conjugated phalloidin (Sigma-Aldrich) was used for F-actin cytoskeleton staining. Fluorescein isothiocyanate–conjugated WGA (5 µg/ml; #L4895, Sigma-Aldrich) was used to visualize t tubules as it binds to sialic acid residues of the cell membrane glycocalyx. This staining is routinely used for the staining of skeletal and cardiac sarcolemma. Nuclei were visualized with 4′,6-

diamidino-2-phenylindole (TCI Chemicals, Tokyo, Japan). Samples were imaged with confocal microscopy (LSM 880, Carl Zeiss, Oberkochen, Germany). Sarcomere lengths were quantified on the basis of α-actinin–stained images using the ZEN program (Carl Zeiss).

Quantitative real-time polymerase chain reaction
The mRNA expression of cardiac markers in CiCMs was quantified by qPCR analysis as previously described (19). Total RNA was extracted from each sample using an RNA extraction kit (Takara, Shiga, Japan). Complementary DNA (cDNA) was synthesized from total RNA using a cDNA synthesis kit (Takara). qPCR was performed using TaqMan Fast Universal PCR Master Mix (Applied Biosystems, Foster City, CA, USA) on a StepOnePlus Real-Time PCR System (Applied Biosystems). The primers used in this study were as follows: mouse *Mef2c* (Mm01340842_m1), mouse *Myh7* (Mm00600555_m1), mouse *Actc1* (Mm01333821_m1), mouse *Nkx2*-5 (Mm01309813_s1), and mouse *Scn5a* (Mm01342518_m1). The relative gene expression levels were quantified on the basis of the cycle threshold (C_t) and normalized to that of the endogenous control gene, mouse *GAPDH* (Mm99999915_g1).

Flow cytometry analysis
To analyze populations of cTnT[+] and α-actinin^{+} cells, cells were harvested by incubation with collagenase IV (1 mg/ml; Thermo Fisher Scientific) for 40 min at 37°C. Samples were then rinsed with cold PBS supplemented with 1% FBS, fixed with 4% paraformaldehyde for 10 min, and permeabilized and blocked with 0.1% Triton X-100 and 5% FBS. The cells were then stained with anti-cTnT (1:200; Thermo Fisher Scientific) or anti–α-actinin (1:500; Sigma-Aldrich), followed by Alexa Fluor 488–conjugated secondary antibody (1:1000; Thermo Fisher Scientific). Flow cytometry was performed using a FACSCalibur flow cytometer (BD Biosciences, Franklin Lakes, NJ, USA). Data were analyzed using FlowJo software (FlowJo, Ashland, OR, USA).

Western blot
To detect the expression of Smad2 and phosphorylated Smad2 (Ser[465/467]), Western blot was performed using our previous protocol (85). Proteins were extracted with radioimmunoprecipitation assay buffer (Sigma-Aldrich) containing a protease inhibitor cocktail (Roche). The primary antibodies used were anti-Smad2 (1:1000 dilution; Cell Signaling Technology), anti-phosphorylated Smad2 (Ser[465/467]) (1:1000 dilution; Cell Signaling Technology), and β-actin (1:2000 dilution; Cell Signaling Technology). Blots were visualized with a Clarity Western ECL Substrate kit (Bio-Rad, Hercules, CA, USA) according to the manufacturer's instructions. Relative expression levels of each target protein were normalized to β-actin controls using ImageJ software.

Calcium imaging
For calcium imaging, cells were stained using 1 to 2 μM Fluo-4 AM (Thermo Fisher Scientific) for 30 min (for 2D samples) or 1 hour (for 3D samples) at 37°C. After washing with cardiac reprogramming basal medium without small molecules, serial images of calcium transients were captured using a confocal microscope (LSM 880, Carl Zeiss). Regions of interest were selected, and changes in fluorescence intensity were analyzed using ZEN software. The changes in calcium transients were monitored with electrical stimulation at a frequency of 1 Hz with 5-V amplitude using a WPG100e electrochemical workstation (WonATech, Seoul, Korea).

Multielectrode array
MEA measurements were performed using the Maestro MEA system with the 12-well MEA plate from Axion BioSystems Inc. (Atlanta, GA, USA). For MEA recording, each beating 3D HEM sample was plated on a fibronectin (50 μg/ml)–coated well of an MEA plate. Before the experiments, all media in the MEA wells were aspirated and exchanged with new media to ensure a known volume of media. The MEA plate was then returned to the incubator for 4 hours to reach an equilibrium. The sampling frequency was set to 12.5 kHz, and the baseline was recorded for 1 min at 5-min intervals for 20 min in total. During the drug testing, MEA signals were likewise recorded for 1 min at 5-min intervals for 20 min in total. Isoproterenol was administered by adding 100 μl (10% total volume of the well) of the prepared 10× samples along the edge of the well. The device automatically adjusted and maintained the temperature and CO_2 level to 37°C and 5%, respectively. The data for the last 1 min recorded during the drug testing (after dose) were analyzed offline using AxIS software (version 2.3.2.4, Axion BioSystems Inc.). Three major parameters were derived from the cardiac field potential in the baseline (control) and post-dose conditions as follows: (i) BPM, (ii) FPA, and (iii) field potential duration corrected using FPDcF (86).

Patch-clamp recording
Whole-cell patch clamp was performed to measure the electrophysiological functions at a single-cell level. 3D HEM CiCMs were dissociated by collagenase IV (1 mg/ml) at 37°C for 50 min, reseeded on 2D HEM (0.05 mg/ml)–coated glass coverslips, and cultured for 4 days. The cells on the coverslips were placed in a recording chamber on an inverted microscope stage and continuously perfused at approximately 3 ml/min with 36.5° ± 1°C bath solution. The APs were recorded with an Axopatch 200B amplifier (Molecular Devices, San Jose, CA, USA) controlled by a Digidata 1440 interface and pClamp software (version 11.3, Molecular Devices). The signals were filtered at a sampling rate of 5 kHz, and they were low-pass–filtered at 1 kHz and stored on a computer. Whole-cell recordings were performed at 37°C using an external solution containing 145 mM NaCl, 5.4 mM KCl, 10 mM Hepes, 1 mM $MgCl_2$, 5 mM glucose, and 1.8 mM $CaCl_2$ (pH adjusted to 7.4) and internal solution containing 120 mM K-Asp, 20 mM KCl, 5 mM NaCl, 2 mM $CaCl_2$, 10 mM Hepes, 5 mM EGTA, and 5 mM Mg–adenosine triphosphate (pH 7.25). We recorded APs of the spontaneous beating cells in the current = 0 mode. All reagents for solution formulation were purchased from Sigma-Aldrich. The following parameters were analyzed: maximum diastolic potential, maximum upstroke velocity (maximum rate of rise of the AP stroke, dV/dt_{max}), beating frequency, and AP amplitude.

Transmission electron microscopy
To examine the sarcomere structures of CiCMs in 3D HEM, cells were fixed with 2% glutaraldehyde and 2% paraformaldehyde in 0.1 M phosphate buffer (pH 7.4) and kept overnight at 4°C. Cells were washed with 0.1 M phosphate buffer and postfixed with 1% osmium tetroxide in 0.1 M phosphate buffer for 2 hours. After dehydration of samples by soaking in an ascending ethanol series (50,

60, 70, 80, 90, 95, and 100%), the samples were infiltrated with propylene oxide for 10 min. Samples were then embedded with a Poly/Bed 812 kit (Polysciences, Warrington, PA, USA) and polymerized in an electron microscope oven (#TD-700, DOSAKA, Kyoto, Japan) at 65°C for 12 hours. TEM images were acquired with a TEM (#JEM-1011, JEOL, Tokyo, Japan) at the acceleration voltage of 80 kV equipped with a Megaview III charge-coupled device camera (Emsis, GmbH, Münster, Germany) in the electron microscopy core facility at Yonsei University College of Medicine.

RNA sequencing analysis
RNA sequencing was performed as previously reported (*87*). The reads were aligned with Tophat (v2.0.13, http://ccb.jhu.edu/software/tophat/) (*88*) to the reference genome (mouse mm10). Cufflinks (v2.2.1, http://cole-trapnell-lab.github.io/cufflinks/papers/) (*88*) was used to calculate gene expression in fragments per kilobase of transcript per million mapped reads. Gene Ontology of Genes and Genomes analysis was then performed for the differentially expressed genes with at least twofold change and $P < 0.05$ using the DAVID program (https://david.ncifcrf.gov/).

MI model and CiCM injection
All animal studies were approved by the IACUC of the Catholic University of Korea (approval number CUMC-2020-0051-01). All animal procedures conformed to the National Institutes of Health guidelines or the guidelines issued by Directive 2010/63/EU of the European Parliament for the protection of animals used in scientific research. Fisher 344 rats (160 to 180 g, 8-week-old males; Koatec, Pyeongtaek, Korea) were anesthetized with 2% inhaled isoflurane and intubated via the trachea with an 18G intravenous catheter. The rats were ventilated with a rodent respirator (Harvard Apparatus, Holliston, MA, USA). A 37°C heating pad was used to maintain the body temperature throughout the operation. The chest was shaved and sterilized with 70% alcohol. MI was induced by permanently ligating the left anterior descending artery with a 7-0 Prolene suture (Ethicon, Somerville, NJ, USA). To establish baseline left ventricular function, EF was examined on postoperation day 7 (inclusion criterion: EF < 45% based on echocardiographic evaluation). The rats were anesthetized again the next day by isoflurane inhalation, intubated, and mechanically ventilated, and their chest was reopened. The animals were randomly assigned to three experimental groups (*n* = 4 per group) as follows: untreated, 2D MAT CiCM injection (1 × 10⁶ cells) or 3D HEM CiCM injection (1 × 10⁶ cells). 3D HEM CiCMs for transplantation were prepared by dissociating the construct into single cells with collagenase IV treatment (1 mg/ml; Thermo Fisher Scientific) for an hour at 37°C. 2D MAT CiCMs for transplantation were collected by trypsinization. No purification step was used to isolate the CiCMs from the 3D HEM construct. The reprogramming efficiency was determined as the ratio of the CiCM number to the total cell number in 3D HEM at 14 days of chemical induction. For cell tracking, 2D MAT CiCMs and 3D HEM CiCMs were labeled with 2 μM Cell-Tracker CM-DiI dye (Thermo Fisher Scientific) by incubating the cells for 20 min at 37°C. Cells in a 50-μl volume were injected at two different sites in the border zone of the infarcted heart. The chest was closed aseptically, and antibiotics and 0.9% normal saline solution were given. All rats received immunosuppressants [azathioprine (2 mg/kg), cyclosporine A (5 mg/kg), and methylprednisolone (5 mg/kg)] daily.

Echocardiography
Animals were anesthetized with 2% isoflurane and placed on a heating pad to maintain the body temperature at 37°C. Serial echocardiography was performed before (baseline) and 1 and 2 weeks after CiCM injection using a transthoracic echocardiography system equipped with a 15-MHz L15-7io linear transducer (Affniti 50G, Philips, Amsterdam, the Netherlands) to determine the EF, FS, LVIDd, LVIDs, SWT, and PWT as follows

$$Vd = [7/(2.4 + LVIDd)] \times LVIDd^3$$
$$Vs = [7/(2.4 + LVIDs)] \times LVIDs^3$$
$$EF\,(\%) = (Vd - Vs)/Vd$$
$$FS\,(\%) = 100 \times (\,LVIDd - LVIDs)/LVIDd$$

where Vd indicates diastolic volume and Vs indicates systolic volume. The echocardiography operator was blinded to the group allocation during the experiment. All measurements were included, with no excluded data.

Hemodynamic measurements
Hemodynamic measurements were performed at the end point 2 weeks before euthanasia. Rats were anesthetized and ventilated as described previously. After thoracotomy without bleeding, the LV apex of the heart was punctured using a 26 G needle, and a 2F conductance catheter (SPR-838, Millar) was inserted into the LV. LV PV parameters were continually recorded using a PV conductance system (MPVS Ultra, ADInstruments, Dunedin, New Zealand) coupled to a digital converter (PowerLab 16/35, ADInstruments). During the measurements, researchers were blinded to the group allocation. Load-independent parameters of cardiac function, including the slopes of the ESPVR and the EDPVR, were measured at different preloads, which were elicited by transient occlusion of the IVC with the needle holder. Fifty microliters of hypertonic saline (20% NaCl) was injected into the left jugular vein to calculate the parallel conductance after hemodynamic measurements. Blood was collected from the LV using the catheter and a heparinized syringe and transferred into cuvettes to convert the conductance signal to volume. The absolute blood volume in the LV was defined by calibrating the parallel conductance and the cuvette conductance. All measurements were included, with no excluded data.

MT staining
Two weeks after CiCM treatment, the rats were euthanized, and the hearts were harvested. The hearts were fixed in 4% paraformaldehyde overnight, embedded in paraffin, and sectioned into 4-μm sections starting at the top of the apex using a microtome (Leica, RM2255, Wetzlar, Germany). The sections were deparaffinized with xylene and fixed in Bouin's solution at 56°C for 90 min. The sections were stained with Weigert's iron hematoxylin solution for 15 min at room temperature and washed with tap water for 15 min. The sections were then stained with Biebrich Scarlet-Acid Fuchsin solution for 15 min at room temperature. Then, the sections were stained with phosphomolybdic acid for 15 min and then with aniline blue for 15 min, followed by incubation in 1% acetic acid for 2 min at room temperature. Washing was performed between each step. Last, the sections were mounted and imaged with Pannoramic MIDI (3DHISTECH, Budapest, Hungary). The percentage

of fibrotic area relative to the entire LV wall area was quantified using ImageJ software with basic add-ons.

Immunohistochemistry

The heart was cross-sectioned into 5-μm sections starting at the top of the apex using a microtome (Leica, RM2255, Germany). After deparaffinization and rehydration, antigen retrieval with a target retrieval solution (DAKO) was performed in a humid chamber. The primary antibodies goat anti-CD31 (1:200; #AF3628, R&D Systems) and mouse anti-cTnT (1:200; #ab8295, Abcam) were used in this study, and the samples were incubated with primary antibodies at 4°C overnight. After washing three times with 1% Tween 20 in PBS, the samples were incubated with secondary antibodies for 90 min at room temperature in the dark. The secondary antibodies used in this study were anti-goat Alexa Fluor 488 (1:500; #A11055, Thermo Fisher Scientific) and anti-mouse Alexa Fluor 488 (1:500; #A21202, Invitrogen). After washing three times with PBS, the sections were mounted on slides with VECTASHIELD mounting medium (#H-1200-10, Vector Laboratories, Newark, CA, USA). The numbers of capillaries and cardiomyocytes were counted in five random microscopic fields using a fluorescence microscope (Nikon, Tokyo, Japan) and presented as per square millimeter of tissue area.

Statistical analysis

All quantitative data are shown as means ± SD. The n numbers stated in the figure legends describe biological replicates. Statistical differences between groups were analyzed by two-tailed unpaired t test using Prism 9 software (GraphPad, La Jolla, CA, USA). For field potential data, statistical analysis was performed using one-way analysis of variance (ANOVA) followed by Dunnett's post hoc test. Results were considered significant when the P value was less than 0.05.

Supplementary Materials

This PDF file includes:
Figs. S1 to S11
Table S1

Other Supplementary Material for this manuscript includes the following:
Movies S1 to S8

View/request a protocol for this paper from *Bio-protocol*.

REFERENCES AND NOTES

1. M. Ieda, J.-D. Fu, P. Delgado-Olguin, V. Vedantham, Y. Hayashi, B. G. Bruneau, D. Srivastava, Direct reprogramming of fibroblasts into functional cardiomyocytes by defined factors. *Cell* **142**, 375–386 (2010).
2. Y.-J. Nam, C. Lubczyk, M. Bhakta, T. Zang, A. Fernandez-Perez, J. McAnally, R. Bassel-Duby, E. N. Olson, N. V. Munshi, Induction of diverse cardiac cell types by reprogramming fibroblasts with cardiac transcription factors. *Development* **141**, 4267–4278 (2014).
3. H. Hirai, N. Katoku-Kikyo, S. A. Keirstead, N. Kikyo, Accelerated direct reprogramming of fibroblasts into cardiomyocyte-like cells with the MyoD transactivation domain. *Cardiovasc. Res.* **100**, 105–113 (2013).
4. R. C. Addis, J. L. Ifkovits, F. Pinto, L. D. Kellam, P. Esteso, S. Rentschler, N. Christoforou, J. A. Epstein, J. D. Gearhart, Optimization of direct fibroblast reprogramming to cardiomyocytes using calcium activity as a functional measure of success. *J. Mol. Cell. Cardiol.* **60**, 97–106 (2013).
5. Y. Fu, C. Huang, X. Xu, H. Gu, Y. Ye, C. Jiang, Z. Qiu, X. Xie, Direct reprogramming of mouse fibroblasts into cardiomyocytes with chemical cocktails. *Cell Res.* **25**, 1013–1024 (2015).
6. C. Huang, W. Tu, Y. Fu, J. Wang, X. Xie, Chemical-induced cardiac reprogramming in vivo. *Cell Res.* **28**, 686–689 (2018).
7. N. Cao, Y. Huang, J. Zheng, C. I. Spencer, Y. Zhang, J. D. Fu, B. Nie, M. Xie, M. Zhang, H. Wang, T. Ma, T. Xu, G. Shi, D. Srivastava, S. Ding, Conversion of human fibroblasts into functional cardiomyocytes by small molecules. *Science* **352**, 1216–1220 (2016).
8. K. Miyamoto, M. Akiyama, F. Tamura, M. Isomi, H. Yamakawa, T. Sadahiro, N. Muraoka, H. Kojima, S. Haginiwa, S. Kurotsu, H. Tani, L. Wang, L. Qian, M. Inoue, Y. Ide, J. Kurokawa, T. Yamamoto, T. Seki, R. Aeba, H. Yamagishi, K. Fukuda, M. Ieda, Direct in vivo reprogramming with Sendai virus vectors improves cardiac function after myocardial infarction. *Cell Stem Cell* **22**, 91–103.e5 (2018).
9. K. Song, Y.-J. Nam, X. Luo, X. Qi, W. Tan, G. N. Huang, A. Acharya, C. L. Smith, M. D. Tallquist, E. G. Neilson, J. A. Hill, R. Bassel-Duby, E. N. Olson, Heart repair by reprogramming non-myocytes with cardiac transcription factors. *Nature* **485**, 599–604 (2012).
10. T. M. Jayawardena, E. A. Finch, L. Zhang, H. Zhang, C. P. Hodgkinson, R. E. Pratt, P. B. Rosenberg, M. Mirotsou, V. J. Dzau, MicroRNA induced cardiac reprogramming in vivo. *Circ. Res.* **116**, 418–424 (2015).
11. L. Qian, Y. Huang, C. I. Spencer, A. Foley, V. Vedantham, L. Liu, S. J. Conway, J.-D. Fu, D. Srivastava, *In vivo* reprogramming of murine cardiac fibroblasts into induced cardiomyocytes. *Nature* **485**, 593–598 (2012).
12. T. M. A. Mohamed, N. R. Stone, E. C. Berry, E. Radzinsky, Y. Huang, K. Pratt, Y.-S. Ang, P. Yu, H. Wang, S. Tang, S. Magnitsky, S. Ding, K. N. Ivey, D. Srivastava, Chemical enhancement of in vitro and in vivo direct cardiac reprogramming. *Circulation* **135**, 978–995 (2017).
13. J. A. Wolfram, J. K. Donahue, Gene therapy to treat cardiovascular disease. *J. Am. Heart Assoc.* **2**, e000119 (2013).
14. D. Biswas, P. Jiang, Chemically induced reprogramming of somatic cells to pluripotent stem cells and neural cells. *Int. J. Mol. Sci.* **17**, 226 (2016).
15. Y. Takeda, Y. Harada, T. Yoshikawa, P. Dai, Chemical compound-based direct reprogramming for future clinical applications. *Biosci. Rep.* **38**, BSR20171650 (2018).
16. G. Testa, M. Russo, G. Di Benedetto, M. Barbato, S. Parisi, F. Pirozzi, C. G. Tocchetti, P. Abete, D. Bonaduce, T. Russo, F. Passaro, Bmi1 inhibitor PTC-209 promotes chemically-induced direct cardiac reprogramming of cardiac fibroblasts into cardiomyocytes. *Sci. Rep.* **10**, 7129 (2020).
17. C. Paoletti, C. Divieto, G. Tarricone, F. Di Meglio, D. Nurzynska, V. Chiono, MicroRNA-mediated direct reprogramming of human adult fibroblasts toward cardiac phenotype. *Front. Bioeng. Biotechnol.* **8**, 529 (2020).
18. V. P. Singh, J. P. Pinnamaneni, A. Pugazenthi, D. Sanagasetti, M. Mathison, K. Wang, J. Yang, T. K. Rosengart, Enhanced generation of induced cardiomyocytes using a small-molecule cocktail to overcome barriers to cardiac cellular reprogramming. *J. Am. Heart Assoc.* **9**, e015686 (2020).
19. Y. Jin, J. S. Lee, J. Kim, S. Min, S. Wi, J. H. Yu, G.-E. Chang, A.-N. Cho, Y. Choi, D.-H. Ahn, S.-R. Cho, E. Cheong, Y.-G. Kim, H.-P. Kim, Y. Kim, D. S. Kim, H. W. Kim, Z. Quan, H.-C. Kang, S.-W. Cho, Three-dimensional brain-like microenvironments facilitate the direct reprogramming of fibroblasts into therapeutic neurons. *Nat. Biomed. Eng.* **2**, 522–539 (2018).
20. J. Sia, P. Yu, D. Srivastava, S. Li, Effect of biophysical cues on reprogramming to cardiomyocytes. *Biomaterials* **103**, 1–11 (2016).
21. S. Min, H.-J. Lee, Y. Jin, Y.-H. Kim, J. Sung, H.-J. Choi, S.-W. Cho, Biphasic electrical pulse by a micropillar electrode array enhances maturation and drug response of reprogrammed cardiac spheroids. *Nano Lett.* **20**, 6947–6956 (2020).
22. Y. Li, S. Dal-Pra, M. Mirotsou, T. M. Jayawardena, C. P. Hodgkinson, N. Bursac, V. J. Dzau, Tissue-engineered 3-dimensional (3D) microenvironment enhances the direct reprogramming of fibroblasts into cardiomyocytes by microRNAs. *Sci. Rep.* **6**, 38815 (2016).
23. S. Kurotsu, T. Sadahiro, R. Fujita, H. Tani, H. Yamakawa, F. Tamura, M. Isomi, H. Kojima, Y. Yamada, Y. Abe, Y. Murakata, N. Akiyama, N. Muraoka, I. Harada, T. Suzuki, K. Fukuda, M. Ieda, Soft matrix promotes cardiac reprogramming via inhibition of YAP/TAZ and suppression of fibroblast signatures. *Stem Cell Rep.* **15**, 612–628 (2020).
24. H. C. Ott, T. S. Matthiesen, S.-K. Goh, L. D. Black, S. M. Kren, T. I. Netoff, D. A. Taylor, Perfusion-decellularized matrix: Using nature's platform to engineer a bioartificial heart. *Nat. Med.* **14**, 213–221 (2008).
25. F. Di Meglio, D. Nurzynska, V. Romano, R. Miraglia, I. Belviso, A. M. Sacco, V. Barbato, M. Di Gennaro, G. Granato, C. Maiello, S. Montagnani, C. Castaldo, Optimization of human myocardium decellularization method for the construction of implantable patches. *Tissue Eng. Part C Methods* **23**, 525–539 (2017).
26. P. M. Crapo, T. W. Gilbert, S. F. Badylak, An overview of tissue and whole organ decellularization processes. *Biomaterials* **32**, 3233–3243 (2011).
27. M.-S. Kim, S. M. Pinto, D. Getnet, R. S. Nirujogi, S. S. Manda, R. Chaerkady, A. K. Madugundu, D. S. Kelkar, R. Isserlin, S. Jain, J. K. Thomas, B. Muthusamy, P. Leal-Rojas, P. Kumar, N. A. Sahasrabuddhe, L. Balakrishnan, J. Advani, B. George, S. Renuse, L. D. N. Selvan,

A. H. Patil, V. Nanjappa, A. Radhakrishnan, S. Prasad, T. Subbannayya, R. Raju, M. Kumar, S. K. Sreenivasamurthy, A. Marimuthu, G. J. Sathe, S. Chavan, K. K. Datta, Y. Subbannayya, A. Sahu, S. D. Yelamanchi, S. Jayaram, P. Rajagopalan, J. Sharma, K. R. Murthy, N. Syed, R. Goel, A. A. Khan, S. Ahmad, G. Dey, K. Mudgal, A. Chatterjee, T.-C. Huang, J. Zhong, X. Wu, P. G. Shaw, D. Freed, M. S. Zahari, K. K. Mukherjee, S. Shankar, A. Mahadevan, H. Lam, C. J. Mitchell, S. K. Shankar, P. Satishchandra, J. T. Schroeder, R. Sirdeshmukh, A. Maitra, S. D. Leach, C. G. Drake, M. K. Halushka, T. S. K. Prasad, R. H. Hruban, C. L. Kerr, G. D. Bader, C. A. Iacobuzio-Donahue, H. Gowda, A. Pandey, A draft map of the human proteome. *Nature* **509**, 575–581 (2014).

28. A. Naba, K. R. Clauser, S. Hoersch, H. Liu, S. A. Carr, R. O. Hynes, The matrisome: *In silico* definition and *in vivo* characterization by proteomics of normal and tumor extracellular matrices. *Mol. Cell. Proteomics* **11**, M111.014647 (2012).

29. C. Lindskog, J. Linné, L. Fagerberg, B. M. Hallström, C. J. Sundberg, M. Lindholm, M. Huss, C. Kampf, H. Choi, D. A. Liem, P. Ping, L. Väremo, A. Mardinoglu, J. Nielsen, E. Larsson, F. Pontén, M. Uhlén, The human cardiac and skeletal muscle proteomes defined by transcriptomics and antibody-based profiling. *BMC Genomics* **16**, 475 (2015).

30. Q. Jallerat, A. W. Feinberg, Extracellular matrix structure and composition in the early four-chambered embryonic heart. *Cell* **9**, 285 (2020).

31. R. Song, L. Zhang, Cardiac ECM: Its epigenetic regulation and role in heart development and repair. *Int. J. Mol. Sci.* **21**, 8610 (2020).

32. M. Lockhart, E. Wirrig, A. Phelps, A. Wessels, Extracellular matrix and heart development. *Birth Defects Res. A Clin. Mol. Teratol.* **91**, 535–550 (2011).

33. M. Rienks, A.-P. Papageorgiou, N. G. Frangogiannis, S. Heymans, Myocardial extracellular matrix. *Circ. Res.* **114**, 872–888 (2014).

34. L. T. Saldin, M. C. Cramer, S. S. Velankar, L. J. White, S. F. Badylak, Extracellular matrix hydrogels from decellularized tissues: Structure and function. *Acta Biomater.* **49**, 1–15 (2017).

35. J. G. Jacot, J. C. Martin, D. L. Hunt, Mechanobiology of cardiomyocyte development. *J. Biomech.* **43**, 93–98 (2010).

36. J. D. Robbins, D. L. Boring, W. J. Tang, R. Shank, K. B. Seamon, Forskolin carbamates: Binding and activation studies with type I adenylyl cyclase. *J. Med. Chem.* **39**, 2745–2752 (1996).

37. J. Bain, L. Plater, M. Elliott, N. Shpiro, C. J. Hastie, H. McLauchlan, I. Klevernic, J. S. Arthur, D. R. Alessi, P. Cohen, The selectivity of protein kinase inhibitors: A further update. *Biochem. J.* **408**, 297–315 (2007).

38. M. Tojo, Y. Hamashima, A. Hanyu, T. Kajimoto, M. Saitoh, K. Miyazono, M. Node, T. Imamura, The ALK-5 inhibitor A-83-01 inhibits Smad signaling and epithelial-to-mesenchymal transition by transforming growth factor-β. *Cancer Sci.* **96**, 791–800 (2005).

39. S. Chen, J. T. Do, Q. Zhang, S. Yao, F. Yan, E. C. Peters, H. R. Schöler, P. G. Schultz, S. Ding, Self-renewal of embryonic stem cells by a small molecule. *Proc. Natl. Acad. Sci.* **103**, 17266–17271 (2006).

40. Y. L. Han, P. Ronceray, G. Xu, A. Malandrino, R. D. Kamm, M. Lenz, C. P. Broedersz, M. Guo, Cell contraction induces long-ranged stress stiffening in the extracellular matrix. *Proc. Natl. Acad. Sci. U.S.A.* **115**, 4075–4080 (2018).

41. N. Sato, L. Meijer, L. Skaltsounis, P. Greengard, A. H. Brivanlou, Maintenance of pluripotency in human and mouse embryonic stem cells through activation of Wnt signaling by a pharmacological GSK-3-specific inhibitor. *Nat. Med.* **10**, 55–63 (2004).

42. S. Wang, L. Ye, M. Li, J. Liu, C. Jiang, H. Hong, H. Zhu, Y. Sun, GSK-3β inhibitor CHIR-99021 promotes proliferation through upregulating β-catenin in neonatal atrial human cardiomyocytes. *J. Cardiovasc. Pharmacol.* **68**, 425–432 (2016).

43. R. Hesselbarth, T. U. Esser, K. Roshanbinfar, S. Schrüfer, D. W. Schubert, F. B. Engel, CHIR99021 promotes hiPSC-derived cardiomyocyte proliferation in engineered 3D microtissues. *Adv. Healthc. Mater.* **10**, 2100926 (2021).

44. N. M. King, M. Methawasin, J. Nedrud, N. Harrell, C. S. Chung, M. Helmes, H. Granzier, Mouse intact cardiac myocyte mechanics: Cross-bridge and titin-based stress in unactivated cells. *J. Gen. Physiol.* **137**, 81–91 (2011).

45. Y. Zhao, P. Londono, Y. Cao, E. J. Sharpe, C. Proenza, R. O'Rourke, K. L. Jones, M. Y. Jeong, L. A. Walker, P. M. Buttrick, T. A. McKinsey, K. Song, High-efficiency reprogramming of fibroblasts into cardiomyocytes requires suppression of pro-fibrotic signalling. *Nat. Commun.* **6**, 8243 (2015).

46. J. L. Ifkovits, R. C. Addis, J. A. Epstein, J. D. Gearhart, Inhibition of TGFβ signaling increases direct conversion of fibroblasts to induced cardiomyocytes. *PLOS ONE* **9**, e89678 (2014).

47. S. Krishtul, L. Baruch, M. Machluf, Processed tissue–derived extracellular matrices: Tailored platforms empowering diverse therapeutic applications. *Adv. Funct. Mater.* **30**, 1900386 (2020).

48. M. L. Lindsey, R. Bolli, J. M. Canty, X.-J. Du, N. G. Frangogiannis, S. Frantz, R. G. Gourdie, J. W. Holmes, S. P. Jones, R. A. Kloner, D. J. Lefer, R. Liao, E. Murphy, P. Ping, K. Przyklenk, F. A. Recchia, L. Schwartz Longacre, C. M. Ripplinger, J. E. Van Eyk, G. Heusch, Guidelines for experimental models of myocardial ischemia and infarction. *Am. J. Physiol. - Heart Circ. Physiol.* **314**, H812–H838 (2018).

49. C. Paoletti, E. Marcello, M. L. Melis, C. Divieto, D. Nurzynska, V. Chiono, Cardiac tissue-like 3D microenvironment enhances route towards human fibroblast direct reprogramming into induced cardiomyocytes by microRNAs. *Cell* **11**, 800 (2022).

50. F. Quondamatteo, D. P. Reinhardt, N. L. Charbonneau, G. Pophal, L. Y. Sakai, R. Herken, Fibrillin-1 and fibrillin-2 in human embryonic and early fetal development. *Matrix Biol.* **21**, 637–646 (2002).

51. A. C. Silva, C. Pereira, A. C. R. G. Fonseca, P. Pinto-do-Ó, D. S. Nascimento, Bearing my heart: The role of extracellular matrix on cardiac development, homeostasis, and injury response. *Front. Cell Dev. Biol.* **8**, 621644 (2021).

52. A. Matsuda, M. R. K. Mofrad, On the nuclear pore complex and its emerging role in cellular mechanotransduction. *APL Bioeng.* **6**, 011504 (2022).

53. K. Wagh, M. Ishikawa, D. A. Garcia, D. A. Stavreva, A. Upadhyaya, G. L. Hager, Mechanical regulation of transcription: Recent advances. *Trends Cell Biol.* **31**, 457–472 (2021).

54. S. Nemec, K. A. Kilian, Materials control of the epigenetics underlying cell plasticity. *Nat. Rev. Mater.* **6**, 69–83 (2021).

55. A. J. Engler, S. Sen, H. L. Sweeney, D. E. Discher, Matrix elasticity directs stem cell lineage specification. *Cell* **126**, 677–689 (2006).

56. B. M. Baker, C. S. Chen, Deconstructing the third dimension: How 3D culture microenvironments alter cellular cues. *J. Cell Sci.* **125**, 3015–3024 (2012).

57. P. Wang, M. Dreger, E. Madrazo, C. J. Williams, R. Samaniego, N. W. Hodson, F. Monroy, E. Baena, P. Sánchez-Mateos, A. Hurlstone, J. Redondo-Muñoz, WDR5 modulates cell motility and morphology and controls nuclear changes induced by a 3D environment. *Proc. Natl. Acad. Sci. U.S.A.* **115**, 8581–8586 (2018).

58. S. R. Caliari, S. L. Vega, M. Kwon, E. M. Soulas, J. A. Burdick, Dimensionality and spreading influence MSC YAP/TAZ signaling in hydrogel environments. *Biomaterials* **103**, 314–323 (2016).

59. J. Baek, P. A. Lopez, S. Lee, T.-S. Kim, S. Kumar, D. V. Schaffer, *Egr1* is a 3D matrix–specific mediator of mechanosensitive stem cell lineage commitment. *Sci. Adv.* **8**, eabm4646 (2022).

60. H. Gerardo, A. Lima, J. Carvalho, J. R. D. Ramos, S. Couceiro, R. D. M. Travasso, R. P. das Neves, M. Grãos, Soft culture substrates favor stem-like cellular phenotype and facilitate reprogramming of human mesenchymal stem/stromal cells (hMSCs) through mechanotransduction. *Sci. Rep.* **9**, 9086 (2019).

61. O. Chaudhuri, L. Gu, D. Klumpers, M. Darnell, S. A. Bencherif, J. C. Weaver, N. Huebsch, H.-P. Lee, E. Lippens, G. N. Duda, D. J. Mooney, Hydrogels with tunable stress relaxation regulate stem cell fate and activity. *Nat. Mater.* **15**, 326–334 (2016).

62. B. Yang, K. Wei, C. Loebel, K. Zhang, Q. Feng, R. Li, S. H. D. Wong, X. Xu, C. Lau, X. Chen, P. Zhao, C. Yin, J. A. Burdick, Y. Wang, L. Bian, Enhanced mechanosensing of cells in synthetic 3D matrix with controlled biophysical dynamics. *Nat. Commun.* **12**, 3514 (2021).

63. H. Shi, C. Wang, Z. Ma, Stimuli-responsive biomaterials for cardiac tissue engineering and dynamic mechanobiology. *APL Bioeng.* **5**, 011506 (2021).

64. B. D. Cosgrove, K. L. Mui, T. P. Driscoll, S. R. Caliari, K. D. Mehta, R. K. Assoian, J. A. Burdick, R. L. Mauck, N-cadherin adhesive interactions modulate matrix mechanosensing and fate commitment of mesenchymal stem cells. *Nat. Mater.* **15**, 1297–1306 (2016).

65. C. K. Miranti, J. S. Brugge, Sensing the environment: A historical perspective on integrin signal transduction. *Nat. Cell Biol.* **4**, E83–E90 (2002).

66. I. A. Janson, A. J. Putnam, Extracellular matrix elasticity and topography: Material-based cues that affect cell function via conserved mechanisms. *J. Biomed. Mater. Res. A* **103**, 1246–1258 (2015).

67. E. Cukierman, R. Pankov, D. R. Stevens, K. M. Yamada, Taking cell-matrix adhesions to the third dimension. *Science* **294**, 1708–1712 (2001).

68. A. D. Doyle, N. Carvajal, A. Jin, K. Matsumoto, K. M. Yamada, Local 3D matrix microenvironment regulates cell migration through spatiotemporal dynamics of contractility-dependent adhesions. *Nat. Commun.* **6**, 8720 (2015).

69. S. Bar, N. Benvenisty, Epigenetic aberrations in human pluripotent stem cells. *EMBO J.* **38**, e101033 (2019).

70. Y. H. Tan, H. R. Helms, K. H. Nakayama, Decellularization strategies for regenerating cardiac and skeletal muscle tissues. *Front. Bioeng. Biotechnol.* **10**, 831300 (2022).

71. S. Das, H. Nam, J. Jang, 3D bioprinting of stem cell-laden cardiac patch: A promising alternative for myocardial repair. *APL Bioeng.* **5**, 031508 (2021).

72. J. S. Lee, Y. S. Choi, J. S. Lee, E. J. Jeon, S. An, M. S. Lee, H. S. Yang, S.-W. Cho, Mechanically-reinforced and highly adhesive decellularized tissue-derived hydrogel for efficient tissue repair. *Chem. Eng. J.* **427**, 130926 (2022).

73. X. Lin, Y. Liu, A. Bai, H. Cai, Y. Bai, W. Jiang, H. Yang, X. Wang, L. Yang, N. Sun, H. Gao, A viscoelastic adhesive epicardial patch for treating myocardial infarction. *Nat. Biomed. Eng.* **3**, 632–643 (2019).

74. J. Shin, S. Choi, J. H. Kim, J. H. Cho, Y. Jin, S. Kim, S. Min, S. K. Kim, D. Choi, S.-W. Cho, Tissue tapes—Phenolic hyaluronic acid hydrogel patches for off-the-shelf therapy. *Adv. Funct. Mater.* **29**, 1903863 (2019).

75. J. S. Lee, Y. H. Roh, Y. S. Choi, Y. Jin, E. J. Jeon, K. W. Bong, S.-W. Cho, Tissue beads: Tissue-specific extracellular matrix microbeads to potentiate reprogrammed cell-based therapy. *Adv. Func. Mater.* **29**, 1807803 (2019).

76. E. Mocan, O. Tagadiuc, V. Nacu, Aspects of collagen isolation procedure. *Curierul Medical* **2**, 3–5 (2011).

77. A.-N. Cho, Y. Jin, Y. An, J. Kim, Y. S. Choi, J. S. Lee, J. Kim, W.-Y. Choi, D.-J. Koo, W. Yu, G.-E. Chang, D.-Y. Kim, S.-H. Jo, J. Kim, S.-Y. Kim, Y.-G. Kim, J. Y. Kim, N. Choi, E. Cheong, Y.-J. Kim, H. S. Je, H.-C. Kang, S.-W. Cho, Microfluidic device with brain extracellular matrix promotes structural and functional maturation of human brain organoids. *Nat. Commun.* **12**, 4730 (2021).

78. J. Cox, N. Neuhauser, A. Michalski, R. A. Scheltema, J. V. Olsen, M. Mann, Andromeda: A peptide search engine integrated into the MaxQuant environment. *J. Proteome Res.* **10**, 1794–1805 (2011).

79. B. Schwanhäusser, D. Busse, N. Li, G. Dittmar, J. Schuchhardt, J. Wolf, W. Chen, M. Selbach, Global quantification of mammalian gene expression control. *Nature* **473**, 337–342 (2011).

80. A. Naba, K. R. Clauser, H. Ding, C. A. Whittaker, S. A. Carr, R. O. Hynes, The extracellular matrix: Tools and insights for the "omics" era. *Matrix Biol.* **49**, 10–24 (2016).

81. M. Uhlén, L. Fagerberg, B. M. Hallström, C. Lindskog, P. Oksvold, A. Mardinoglu, Å. Sivertsson, C. Kampf, E. Sjöstedt, A. Asplund, I. Olsson, K. Edlund, E. Lundberg, S. Navani, C. A.-K. Szigyarto, J. Odeberg, D. Djureinovic, J. O. Takanen, S. Hober, T. Alm, P.-H. Edqvist, H. Berling, H. Tegel, J. Mulder, J. Rockberg, P. Nilsson, J. M. Schwenk, M. Hamsten, K. von Feilitzen, M. Forsberg, L. Persson, F. Johansson, M. Zwahlen, G. von Heijne, J. Nielsen, F. Pontén, Proteomics. Tissue-based map of the human proteome. *Science* **347**, 1260419 (2015).

82. H. Mi, A. Muruganujan, D. Ebert, X. Huang, P. D. Thomas, PANTHER version 14: More genomes, a new PANTHER GO-slim and improvements in enrichment analysis tools. *Nucleic Acids Res.* **47**, D419–D426 (2019).

83. Y. Jin, J. Kim, J. S. Lee, S. Min, S. Kim, D.-H. Ahn, Y.-G. Kim, S.-W. Cho, Vascularized liver organoids generated using induced hepatic tissue and dynamic liver-specific microenvironment as a drug testing platform. *Adv. Func. Mater.* **28**, 1801954 (2018).

84. G. Park, B. S. Yoon, Y. S. Kim, S.-C. Choi, J.-H. Moon, S. Kwon, J. Hwang, W. Yun, J.-H. Kim, C.-Y. Park, D. S. Lim, Y. I. Kim, C. H. Oh, S. You, Conversion of mouse fibroblasts into cardiomyocyte-like cells using small molecule treatments. *Biomaterials* **54**, 201–212 (2015).

85. Y. Jin, J.-U. Lee, E. Chung, K. Yang, J. Kim, J.-W. Kim, J. S. Lee, A.-N. Cho, T. Oh, J.-H. Lee, S.-W. Cho, J. Cheon, Magnetic control of axon navigation in reprogrammed neurons. *Nano Lett.* **19**, 6517–6523 (2019).

86. B. Vandenberk, E. Vandael, T. Robyns, J. Vandenberghe, C. Garweg, V. Foulon, J. Ector, R. Willems, Which QT correction formulae to use for QT monitoring? *J. Am. Heart Assoc.* **5**, e003264 (2016).

87. Y. Jin, E. J. Jeon, S. Jeong, S. Min, Y. S. Choi, S. H. Kim, J. S. Lee, J. Shin, J. H. Yu, D.-H. Ahn, Y.-G. Kim, H. S. Yang, T. J. Kang, S.-R. Cho, N. Choi, S.-W. Cho, Reconstruction of muscle fascicle-like tissues by anisotropic 3D patterning. *Adv. Func. Mater.* **31**, 2006227 (2021).

88. C. Trapnell, A. Roberts, L. Goff, G. Pertea, D. Kim, D. R. Kelley, H. Pimentel, S. L. Salzberg, J. L. Rinn, L. Pachter, Differential gene and transcript expression analysis of RNA-seq experiments with TopHat and Cufflinks. *Nat. Protoc.* **7**, 562–578 (2012).